2019

PALEOMAGNETIC INVESTIGATION OF IGNEOUS ROCKS DEFORMED BY THE KEWEENAW FAULT IN THE NORTHWESTERN KEWEENAW PENINSULA.

Daniel Trekas

PALEOMAGNETIC INVESTIGATION OF IGNEOUS ROCKS DEFORMED BY THE KEWEENAW FAULT IN THE NORTHWESTERN KEWEENAW PENINSULA.

By

Daniel B. Trekas

A THESIS

Submitted in partial fulfillment of the requirements for the degree of

MASTER OF SCIENCE

In Geophysics

MICHIGAN TECHNOLOGICAL UNIVERSITY

2019

This thesis has been approved in partial fulfillment of the requirements for the Degree of MASTER OF SCIENCE in Geophysics.

Department of Geological and Mining Engineering and Sciences

Thesis Advisor:	*Aleksey Smirnov*
Committee Member:	*Chad Deering*
Committee Member:	*James DeGraff*
Department Chair:	*John Gierke*

Table of Contents

List of Figures

List of Tables

Acknowledgments

I would like to thank my advisor Aleksey Smirnov and committee members Chad Deering and James DeGraff for all there help and advice throughout my research.

I would like to thank all those who helped me with my research.

All those who have helped me with lab work:

Katie Bristol, Marine Foucher, Sonia Jin, and Adren Rigdon

All those who have helped me with sample collection:

Graham Hubbell, Elisa Piispa, Leonid Surovitckii, and Colin Tyrrell

Property owners of sample sites for allowing me to sample:

Chuck Brumleve, Hal Baldauf, Gina Nicholas, Frank Nicholas, and The Keweenaw Community Forest Company

Lastly, I would like to thank my friends and family for all the support during my education and research.

Abstract

One of the most prominent structural features associated with the ~1.1 Ga Midcontinent Rift (MCR) system is the >350 km long Keweenaw Fault that bisects the Keweenaw Peninsula, separating the MCR-related Portage Lake Volcanics (PLV) and the younger Jacobsville Sandstone (JS). The fault trend is NE-NNE over most of its length, but changes to an easterly direction along the shore of Bête Grise Bay near the end of the peninsula. Conventionally, the Keweenaw Fault has been considered to be a continuous reverse (dip-slip) fault formed by inversion of an original rift-bounding normal fault during the Grenville Orogeny. However, recent mapping shows that the fault in this area is not a single continuous feature but instead is a fault system consisting of ENE and ESE-trending segments with substantial strike-slip movement. This segmented fault geometry could have resulted in local folding of PLV and JS strata adjacent to the fault segments. To test this hypothesis, a paleomagnetic investigation was conducted on samples of PLV basaltic flows from eight sites in the Lake Medora and Fort Wilkins map quadrangles. The sites represent the opposite flanks of a proposed anticline with an ESE-trending axis. All eight sites yielded reliable and consistent site-mean directions of characteristic remanent magnetization (ChRM). A paleomagnetic fold test conducted on these sites showed that after unfolding the ChRM directions are similar to the paleomagnetic direction expected from unfolded PLV rocks. Data from two sites also suggest rotations around a vertical axis consistent with strike-slip movement. Paleomagnetic directions obtained from three additional sites with brecciated PLV basalt and JS sandstone as well as a clastic dike of JS cutting PLV, are randomized within each site. These randomized directions provide additional evidence that paleomagnetic data from the PLV basalts were not affected by a later remagnetization event. Overall, the paleomagnetic results support the hypothesis of fault-induced folding of PLV strata in the study area. In addition, this research demonstrates that paleomagnetism represents a useful tool to investigate local structural deformation within the MCR system.

1.0 Introduction

1.1 Midcontinent Rift System

The North American Midcontinent Rift (MCR) system represents a failed rifting event that occurred within the North American plate (Laurentia craton) about 1.1 billion years (Ga) ago (e.g., Ojakangas et al., 2001) (Figure 1). The MCR system is the only Precambrian rift system that is well-preserved and thus provides a unique opportunity to investigate significant problems of Mesoproterozoic plate tectonics and geodynamics. Outcrops of MCR- related rocks are only exposed in the Lake Superior region. However, strong magnetic and gravity anomalies indicate that the MCR system extends from NE Kansas northward to Lake Superior and through Michigan and NE Ohio.

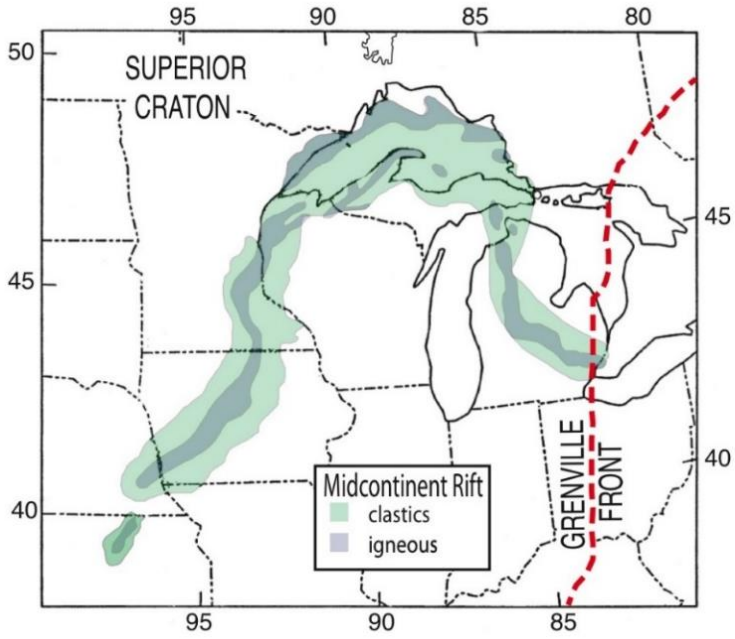

Figure 1. Map showing the extent of the Midcontinent Rift System (Huber, 1973).

Rift-related magmatism resulted in eruption of >300,000 km^3 of predominantly mafic, mantle-derived magma and emplacement of possibly an equal amount of intrusive rocks (Green et al., 1987; Cannon et al., 1989; Hutchinson et al., 1990; Davis and Green, 1997). Based on high-precision U-Pb geochronology data, MCR magmatic activity is divided into a precursor stage (~1145–1140 Ma), two main pulses (~1115–1105 Ma and ~1100–1094 Ma), and a period of diminishing volcanic activity (1087–1085 Ma) (e.g., Davis and Green, 1997; Heaman et al., 2007; Kulakov et al., 2014).

The Midcontinent Rift evolved from widespread but localized magmatism during the early stage of rifting to more intense magmatism within the down-dropped rift graben during the main stage, followed by sedimentary infilling during the post-rift sag phase (Bornhorst and Lankton, 2009). Initiation of rifting was likely associated with an ascending mantle plume spreading laterally at the base of the crust (Ernst and Bell, 2010; Platt and Mitchell, 1979) causing the crust to break and separate along inwardly dipping, normal faults (Figure 3). The oldest igneous rocks of the MCR system include intrusive rocks of the Logan sills dated at 1109-2+4 Ma (Davis and Suttclife, 1985) and the layered series of the Duluth Complex dated at 1106.9 ± 0.6 Ma (Paces and Miller, 1992), both located in the northwestern part of the Lake Superior region (Figure 2). Recent paleomagnetic data indicate that some E-W trending mafic dikes in Baraga and Marquette counties may also represent the early stage of the MCR (Foucher, 2018).

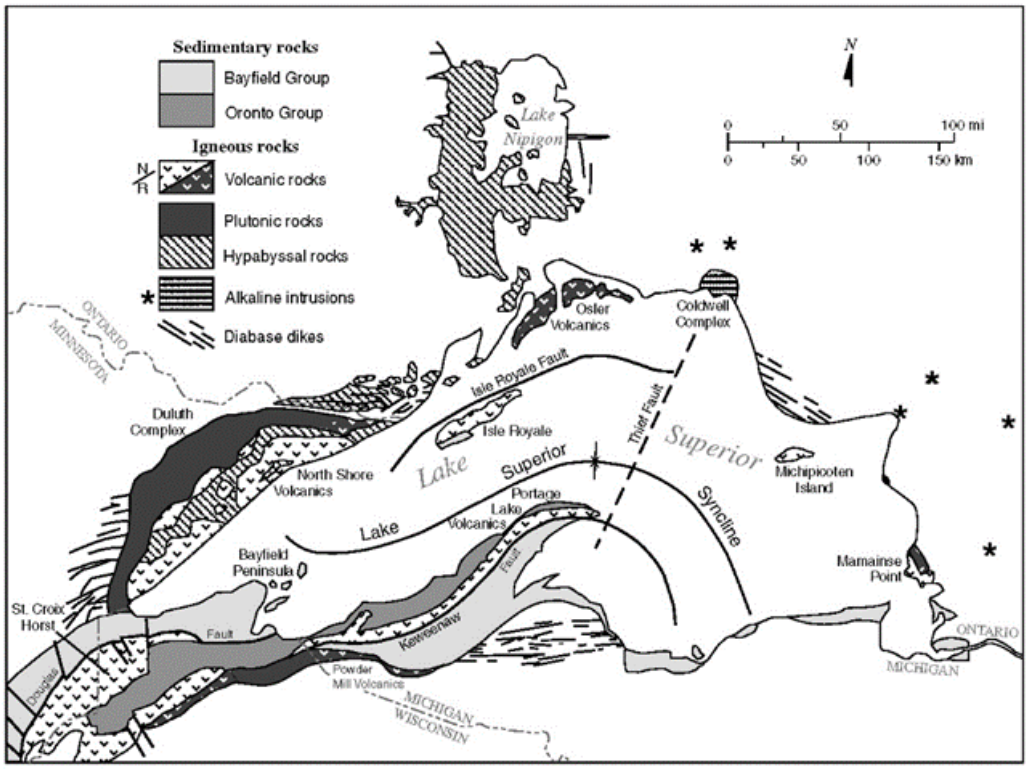

Figure 2. Generalized geologic map of the Lake Superior basin (N/R indicates normal/reversed magnetic polarity) (Ojakangas et al., 2001).

The main stage of rifting was associated with eruption of large volumes of mantle-derived mafic magma and lesser amounts of felsic magma over the subsiding Archean and Paleoproterozoic crust (Green et al., 1987; Cannon et al., 1989; Hutchinson et al., 1990; Davis and Green, 1997). Along the Keweenaw Peninsula, these magmas formed a thick succession of basaltic flows and rhyolitic domes known as the Portage Lake Volcanics (PLV) (Section 1.2). Between eruption episodes, periods of erosion and weathering were sometimes long enough for sedimentary units to be deposited between the flows. Ten named conglomerates, including the Allouez and the

St. Louis conglomerates, and three named sandstone units are useful markers for stratigraphic correlations along the Keweenaw Peninsula.

Emplacement of the PLV was followed by continued sagging of the rift basin due to the weight of overlying rocks and the plastic nature of previously melted crust underlying the rift, further establishing the Superior Syncline and forming the western part of Lake Superior (Cannon et al., 1989). While basin subsidence was occurring, transport of erosional and weathering products filled the basin with almost 8 km of clastic sediments. In the Keweenaw Peninsula, the PLV is overlain by the Copper Harbor Conglomerate (CHC) consisting mostly of coarse alluvial conglomerate and lava flows of the 1087 Ma Lake Shore Traps, representing the last significant MCR-related magmatic event in this area (Davis and Paces, 1990). The CHC is conformably overlain by the Nonesuch Formation and Freda Sandstone.

After 50 million years of rift evolution, rifting and associated magmatic activity ended without breaking Laurentia (Cannon et al., 1989). The last major tectonic event to affect the MCR was continental collision that culminated at about 1060 Ma but could have started as early as 1080 Ma (Cannon, 1994). This event is related to renewed northwest-directed compression from the Grenville Orogeny, which inverted the original rift-bounding normal faults into reverse faults (Cannon, 1994). During this time, the limbs of the Lake Superior Syncline broke along the Keweenaw and Isle Royale faults. The northwestern and southeastern limbs now form Isle Royale and the Keweenaw Peninsula, exposing MCR rocks related to the main and late stages of the rift activity (Figure 3).

The Keweenaw Fault represents one of the most prominent structural features associated with the MCR system. The fault can be traced for about 350 km, trending NE-NNE from northern Wisconsin to the end of the Keweenaw Peninsula, where the fault curves to an easterly direction along the Bête Grise Bay shore (Cannon and Nicholson, 2001). According to geophysical data, the fault may continue into Lake Superior, further changing its trend to southeast (Ojakangas et al., 2001). The conventional interpretation is that the Keweenaw Fault is a continuous reverse fault formed by inversion of a rift-bounding normal fault.

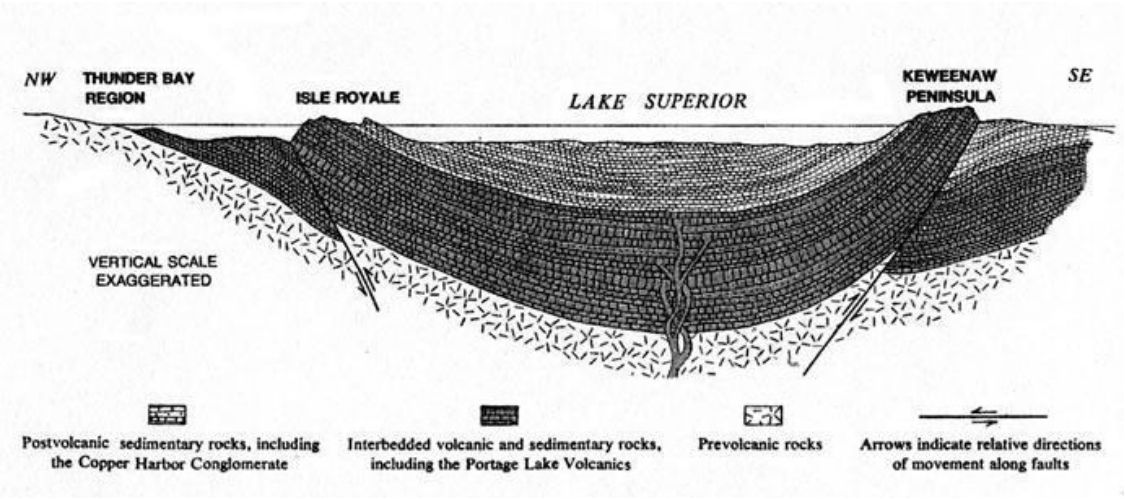

Figure 3. Schematic cross-section of the Lake Superior Basin with the conventional interpretation of the Keweenaw and Isle Royale Faults (Huber, 1975).

However, new research at Michigan Tech indicates that the conventional interpretation is not consistent with fault geometry and field observations (Tyrrell et al., 2018). Instead, new mapping suggests that the Keweenaw Fault is a discontinuous fault system consisting of (1) ESE-trending en echelon segments with SE-trending splays,

and (2) ENE-trending segments that appear to connect with the former to create a zigzag pattern (DeGraff, 2018). In addition, field data indicate a substantial strike-slip component of motion. The observed folding of PLV and JS strata adjacent to the fault may reflect accommodation to this type of fault geometry and evolution.

The main objective of this project is to test this hypothesis of folding related to the newly mapped fault system using paleomagnetic data from PLV rocks. Obtained paleomagnetic directions are rotated on horizontal axes to their inferred initial positions using dip azimuth and plunge of the basaltic flows measured in the field. Paleomagnetic directions thus rotated are then compared with the well-known reference paleomagnetic direction of PLV rocks to test whether the unfolding correction is consistent with the fold hypothesis.

1.2. The Portage Lake Volcanics

The ~1095 Ma Portage Lake Volcanics (PLV) along the Keweenaw Peninsula erupted over a period of 2 to 3 million years (Davis and Paces, 1990). These tholeiitic flood basalts erupted into a subsiding rift basin from a fissure system located near the center of present-day Lake Superior (White, 1960). Stratigraphically upwards, the PLV exhibit a trend to more-primitive magma compositions with negligible crustal contamination in the youngest flows (Paces, 1988). The PLV have been divided into two groups based on their TiO_2 content. The low-TiO_2 basalts make up to 90% of all PLV.

The total thickness of PLV flows and interflow sediments is about 3-5 km (Paces, 1988). The PLV on the Keweenaw Peninsula is characterized by considerable changes in dip azimuths and dip angles along the strike of the peninsula, reflecting the curvature of the MCR. Moving from west to east along the peninsula, dip directions systematically vary from northwest near Houghton to northeast at the eastern tip of the peninsula. Some PLV flows can be traced for 30-50 km along strike, with a few that can be traced ~100 km. The Greenstone Flow near the PLV top has been dated to 1094 ± 1.5 Ma (Davis and Paces, 1990), and the Copper City Flow near the PLV bottom has been dated to 1096 ± 1.8 Ma (Davis and Paces, 1990).

During post-rift compression between 1060 and 1047 Ma (Bornhorst et al., 1988; Browning and Beske-Diehl, 1987), upward movement of burial metamorphic hydrothermal fluids resulted in alteration of rift-filling rocks and formation of native copper deposits (Bornhorst, 1997). These hydrothermal fluids also caused formation of hematite in vesicular and permeable flow tops of the PLV (Browning and Beske-Diehl, 1987). Less permeable massive flow interiors remained relatively fresh and unaltered.

This study focused on the paleomagnetic investigation of PLV flows exposed on the Keweenaw Peninsula and adjacent to the Keweenaw Fault. Most previous paleomagnetic investigations of the PLV were done more than 25 years ago (e.g., DuBois, 1962; Vincenz and Yaskawa, 1968; Books, 1968; 1972) and do not meet modern reliability criteria of paleomagnetic research. Later studies focused on copper mineralization (Browning and Beske-Diehl, 1987; Li and Beske-Diehl, 1993), basaltic lava flows in the Quincy Mine (Michels, 2013), or Midcontinent Rift curvature in the

Lake Superior region (Hnat et al., 2006) (Table 1). Recently, a detailed paleomagnetic investigation of 74 PLV flows at the tip of the Keweenaw Peninsula (Kulakov, 2014) isolated a primary remanent magnetization carried by magnetite or low-Ti titanomagnetite between ~525°C and 585°C. The group-mean direction for this primary component is D=289.8°, I=36.9°, α_{95}=8.2° (D – declination, I – inclination, α_{95} - the 95% radius of confidence). The computed angular dispersion of virtual geomagnetic poles (S = 12.7 ± 2.1°, N=65) is statistically similar to the value of S = 12° (λ_{paleo} = 21°) calculated for the 1.0-2.2 Ga interval (Smirnov et al., 2011). Therefore, these paleomagnetic data adequately represent a time-averaged geomagnetic field. In this study, the paleomagnetic direction reported by Kulakov (2014) is used as a reference paleomagnetic direction for unfolded PLV flows.

Study	Formation	D(°)	I(°)	α_{95}(°)	k	N
DuBois (1962)	PLV	282.5	44.0	4.0	47.2	31*
Vincenz (1968)	PLV	286.0	33.0	9.0	NL	14
Books (1968)	PLV	NL	NL	2.6	105.8	29*
Books (1972)	PLV 1	287.7	26.2	10.8	51.5	5
	PLV 2	284.2	30.9	5.0	332.7	4
	PLV 3	291.0	34.9	3.1	105.5	22
	PLV 4	274.5	45.8	7.1	72.9	7
	PLV 5	289.3	35.1	3.5	77.1	23
	PLV 6	288.4	36.4	7.0	27.2	17
Browning and Beske-Diehl (1987)	PLV	291.4	25.9	13.2	50.0	92*
Michels (2013)	PLV magnetite NC	286.8	35.0	2.4	104.0	32
	PLV magnetite C	287.6	34.0	3.5	85.2	19
	PLV hematite NC	286.5	39.8	3.0	91.6	29
	PLV hematite C	284.0	39.7	4.4	77.3	17
Kulakov (2014)	PLV	289.8	36.9	8.2	41.0	65

Table 1. Paleomagnetic results obtained from the Portage Lake Volcanics. D - declination: I - inclination; α95 - radius of the 95% confidence circle; k is the precision parameter (Fisher, 1953), N is the number of sites, *samples, NL= not listed.

1.3. Site Descriptions

Samples for paleomagnetic research presented here were collected from eleven sites (PM01-11) near the Keweenaw Fault along the shore of Bête Grise Bay in the Lake Medora and Fort Wilkins map quadrangles (Figure 4, Table 2). An additional nine sites (PM12-20) collected in the same area (Figure 4) have not been investigated in this study.

Sites PM01-05 and PM09-11 sample basaltic PLV flows (Figure 5). Structural interpretations described below are based on work by J. DeGraff and his students (DeGraff, 2018; Tyrell et al., 2018). North-dipping flows at sites PM01, PM04, and PM05 represent one structural domain (Domain A) defined as a group of sites with a similar structural rotation. Together with the north-dipping flow at site PM10 (Domain B), they may represent either the north flank of a single EW-trending anticline or the northern flanks of two parallel anticlines separated by a fault (J. DeGraff, personal communication). South-dipping flows at sites PM09 and PM11 (Domain C) represent the south flank of the same anticline containing PM10 on its north flank. Southeast-dipping sites PM02 and PM03 (Domain D) represent the same anticline as sites PM9-11; however, they are near the plunging axis where layer strike is different from the other sites. Their dip azimuth is SE, whereas it is SSE at PM09 and PM11.

Sites PM06 and PM07 sample sandstone and basalt from different parts of a fault breccia zone, and site PM08 samples a clastic dike interpreted to be injected during fault movement.

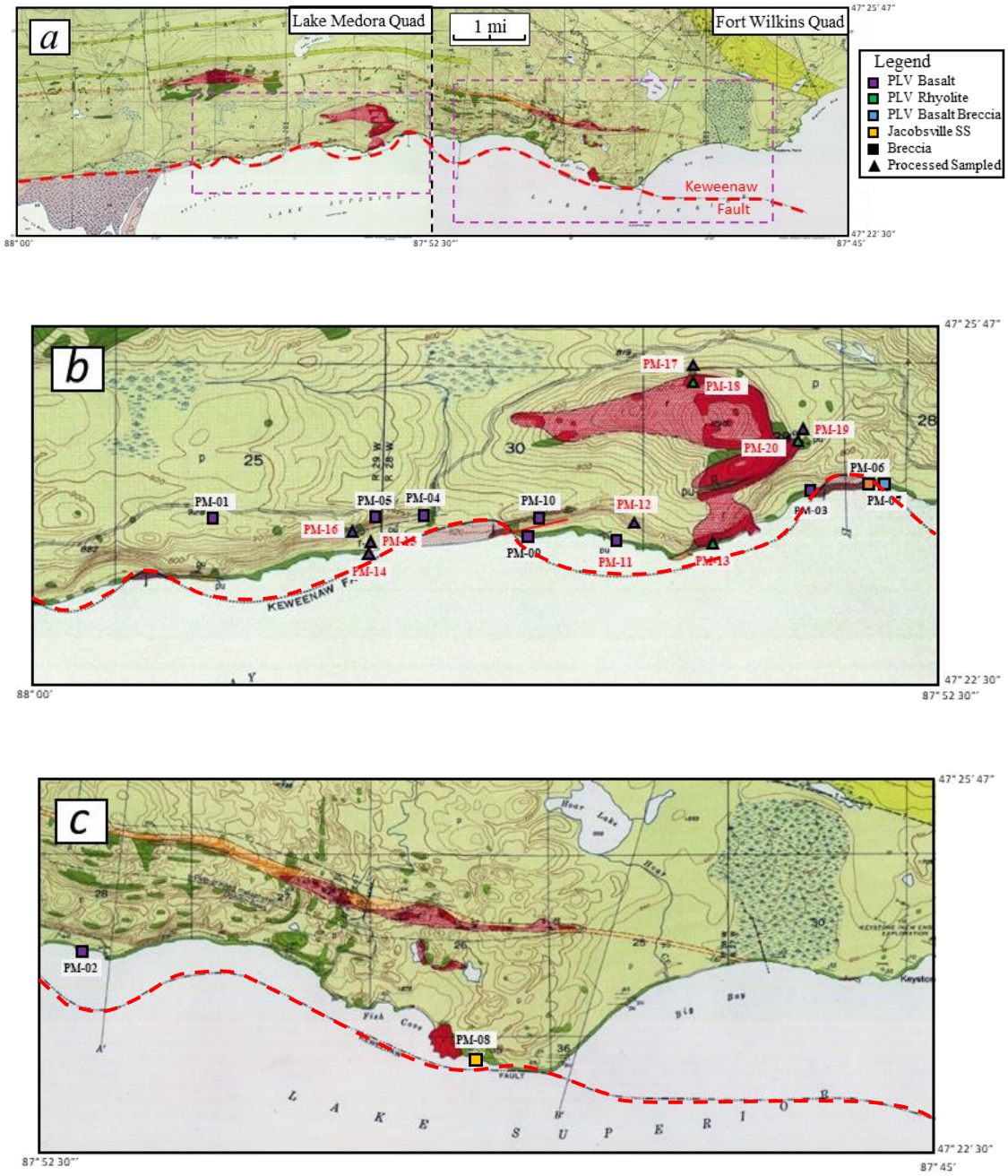

Figure 4. Map of the study area. (a) Lake Medora and Fort Wilkins map quadrangles. The Keweenaw Fault is shown by the red dashed line. (b) and (c) sample locations and rock types of sites PM01-PM20 (Cornwall, 1954).

SITE	Lat (°)	Long (°)	Dip A (°)	P (°)	UR/OT	N
PM-01	47.39362	87.93348	182	75	OT	19
PM-02	47.39445	87.86982	152	30	UR	7
PM-03	47.39508	87.88588	129	38	UR	8
PM-04	47.39380	87.91665	357	87	UR	9
PM-05	47.39375	87.91988	358	84	UR	7
PM-06	47.39568	87.88038	N/A	N/A	UR	6
PM-07	47.39568	87.88033	N/A	N/A	UR	4
PM-08	47.38592	87.82342	N/A	N/A	UR	1
PM-09	47.39297	87.90767	152	80	UR	6
PM-10	47.39383	87.90408	345	75	UR	7
PM-11	47.39278	87.90157	168	76	UR	6

Table 2. Sampled sites. Lat, Long: site coordinates; Dip A: Dip Azimuth, P: Plunge, UR/OT: upright/overturned outcrop; N: Number of sampled cores.

Figure 5. Images of sampled outcrops of PLV basalt at sites PM01-PM04.

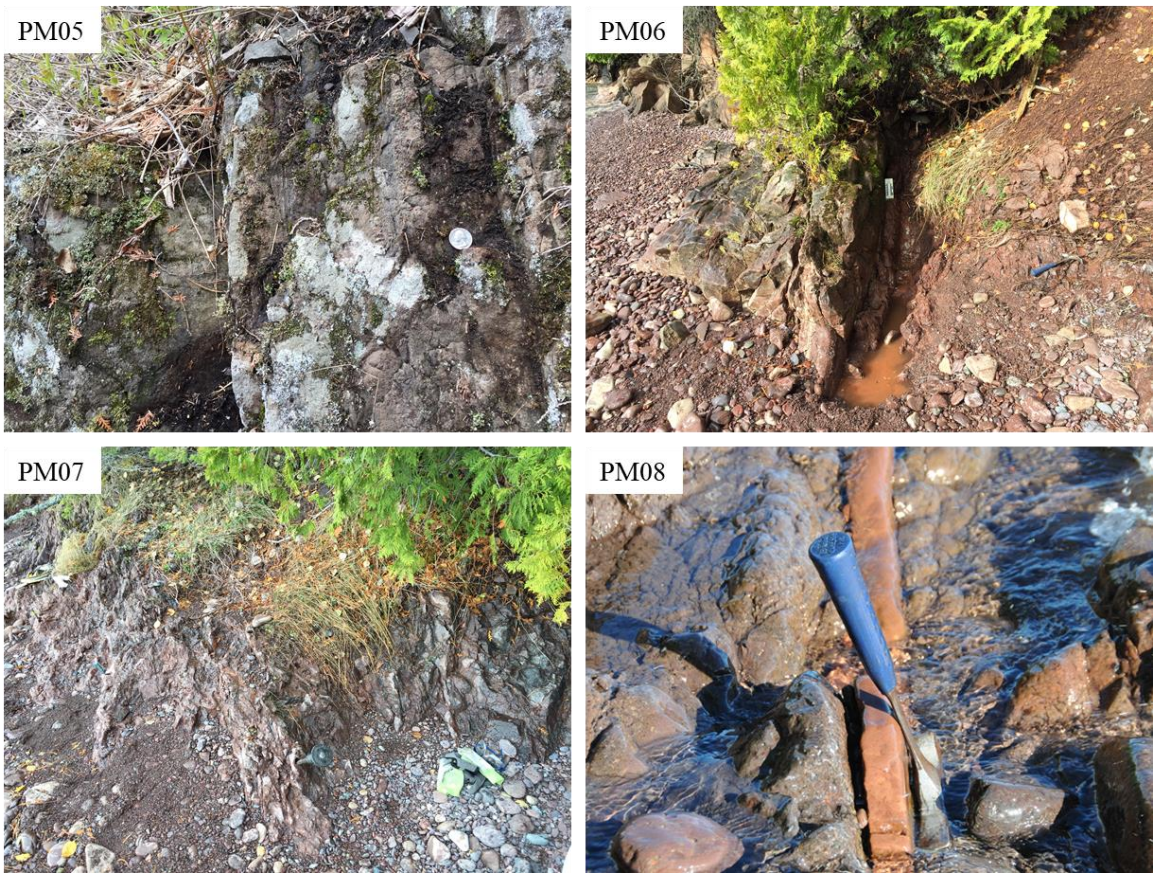

Figure 5 cont. Images of sampled outcrops of PLV basalt (PM05), JS fault breccia (PM06), PLV fault breccia (PM07), and a JS clastic dike (PM08).

2.0 Methods

2.1 Sample Collection

Twenty sites (PM01-PM20) were sampled with a minimum of six independently oriented cores per site. The sampling sites were checked for the presence of a lightning-induced isothermal remanent magnetization (IRM) at topographic highs. This was accomplished by checking if a magnetic compass needle was deflected by ≥5° when the compass was moved vertically down from a ~1-meter height to the outcrop surface. In the

case of a noticeable deflection, the spot was not used for sampling. The cores were collected using a Pomeroy Model D261-C power drill and BSS-1E drill bit. The cores were oriented using a Pomeroy Orienting Fixture clinometer and Brunton Compass; the magnetic azimuth, sundial, and hade of the borehole were measured for each core (Figure 6). The bedding down-dip azimuth and dip angles of the sampled PLV lava flows were also measured at each site (Table 2).

Cylindrical specimens 13 mm in height and 15 mm in diameter were cut from each core to be used for thermal demagnetization (Section 2.2). In addition, 300-500 mg of each core was crushed to a fine powder for thermomagnetic analysis (Section 2.3). Small chips of each core were made for magnetic hysteresis analyses approximately 1 mm^3 (Section 2.4). To avoid weathering alterations, all the specimens were prepared from the bottom of each core.

Figure 6. The Pomeroy Orienting fixture with a Brunton compass used to orient the core samples.

2.2 Thermal Demagnetization

Magnetic remanence measurements were conducted using a 2G Enterprises 760-R superconducting rock magnetometer (SRM) in a magnetically shielded room (Figure 7). Before measurements, the SRM software (PAcquire v.3.70) was used to create a special file for each specimen. The file contains information about the specimen volume and the core orientation along with the plunge and bearing of outcrop the sample was drilled from. The software used this information to convert the measured remanence directions to the geographical coordinates automatically.

Figure 7. The 2G Enterprise 760-R superconducting rock magnetometer in Michigan Tech's Earth Magnetism Laboratory.

After measurement of their natural remanent magnetization (NRM), specimens were cycled through the Verwey transition at ~120 K (Verwey, 1939) by immersing them

into liquid nitrogen to reduce a viscous magnetization component carried by larger magnetite grains (Schmidt, 1993). After the low-temperature demagnetization procedure, samples were put through a series of heating steps to thermally demagnetize their NRM using an ASC TD-48SC thermal specimen demagnetizer flushed with nitrogen gas (Figure 8). Thermal demagnetization was performed until the samples' magnetic intensity was reduced to noise levels or becomes too erratic.

Figure 8. The ASC TD-48SC thermal specimen demagnetizer in Michigan Tech's Earth Magnetism Laboratory.

Twenty-three demagnetization steps were performed on a set of specimens representing all the samples. To increase the confidence in the obtained results, for many samples, a second specimen was thermally demagnetized with a reduced number (10-12) of temperature steps within the unblocking temperature range of their characteristic remanent magnetization (ChRM). After each temperature step, the X, Y, and Z

components of the remaining magnetic remanence measured by the SRM were automatically re-calculated by the PAcquire v.3.70 software into the total moment and magnetization, as well as the declination and inclination in the core, bedding, and geographic coordinates. The measured paleomagnetic data were processed using the PaleoMag v 3.1b1 software. The demagnetization data were plotted on vector end-point and equal area plots for visual inspection and identification of magnetization components (Figure 9).

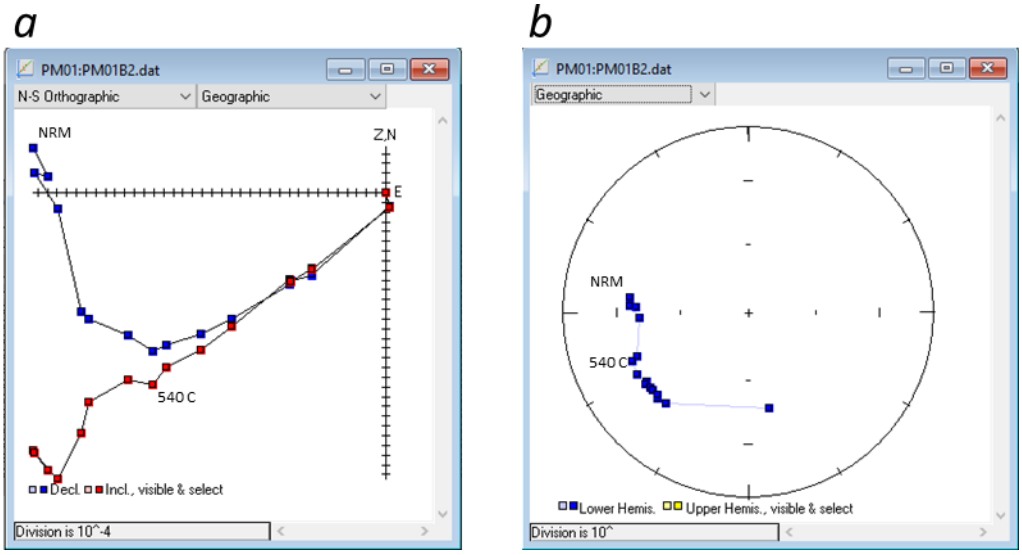

Figure 9. Examples of demagnetization behavior measured from a site PM01 sample. (a) Vector end-point diagram (red/blue symbols show the endpoint projections on vertical/horizontal plane). (b) Equal-area plot showing the directions of magnetic remanence after each demagnetization step. NRM=Natural Remanent Magnetization.

Most measured samples showed a two-component NRM (Figure 9a). A "soft" low-temperature component was typically removed by 500-540 °C. The characteristic

remanent magnetization (ChRM) component was identified by a straight linear demagnetization trajectory toward the origin on a vector end-point diagram (Figure 9a).

The remanence directions were calculated using the principal component analysis on linear segments of the demagnetization trajectories (Kirschvink, 1980). The best-fit line was used if it was defined by at least four successive demagnetization steps with less than 10° maximum angular deviation (MAD). The ChRM directions were then averaged at the site level using Fisher statistics (Fisher, 1953).

2.3 Thermomagnetic Analyses

To analyze the magnetic mineral composition, an AGICO MFK-1FA magnetic susceptibility meter (Kappabridge) with a CS-3 Furnas Apparatus and a CS-L cryostat was used (Figure 10). The 300-500 mg powdered samples are placed into a quartz tube with a thermocouple to measure the temperature of the samples. Each sample underwent three temperature steps.

First, the sample is cooled to approximately -192°C using the cryostat and liquid nitrogen for the initial low-temperature step. Once the sample was cooled to this temperature, all excess liquid nitrogen was flushed from the system using argon to avoid oxidation. The samples' magnetic susceptibility was then measured by the Kappabridge as the sample was heated back to 0°C. The next high-temperature step used the CS-3 Furnace Apparatus. The sample was heated to approximately 700°C at 5°C steps in the argon flushed furnace to avoid oxidation. The sample was then measured as it cooled back to room temperature. The second low-temperature step followed the same procedure as

the first. The cryostat was replaced, and the sample was cooled back to approximately -192°C and measured as it heated back to room temperature.

The low and high-temperature thermomagnetic curves were corrected by subtracting the empty Cryostat and Furnace curves. The data were then normalized by the specimen mass. These corrections were done using the Cureval 8.0.2 software. These corrected thermomagnetic curves were used to identify magnetic minerals based on Curie temperature analysis.

Figure 10. The AGICO MFK1-FA Kappabridge in the Michigan Tech Earth Magnetic Laboratory.

2.4 Magnetic Hysteresis Analyses

Magnetic hysteresis measurements were conducted with a MicroMag Model 2900 Alternating Gradient Field Magnetometer (AGFM) (Figure 11). The AGFM measures both induced and remanent magnetic moments imparted in a specimen as a function of

the applied magnetic field strength (Graham, 2000). Magnetic hysteresis measurements are used to evaluate the magnetic domain state and grain-size distribution, and to identify magnetic mineral phases in a sample.

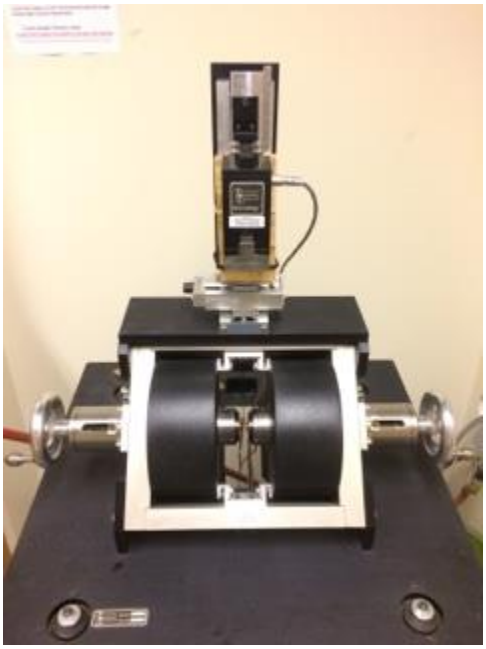

Figure 11. The MicroMag Model 2900 Alternating Gradient Field Magnetometer (AGFM) in Michigan Tech's Earth Magnetism Laboratory.

For measurement, a small specimen (rock chip) is placed on the AGFM sample holder stage (about 3 x 3 mm^2 in size) using a small amount of diamagnetic silicone grease (Dow Release Compound 7) as adhesive. Next, the specimen is placed between the poles of a water-cooled electromagnet that can create magnetic fields within a -1.4 to 1.4 Tesla range. The applied field intensity is measured by a Hall probe. The AGFM has two additional gradient field coils that create a periodically varying gradient magnetic field in the specimen region to vibrate the specimen. The amplitude of this vibration, proportional

to the specimen's magnetic moment, was measured by a piezoelectric transducer built-in the sample holder.

Before each measurement, the sample holder stage was cleaned with isopropanol to remove any possible contaminants. The AGFM was calibrated using an yttrium iron garnet sphere standard with a magnetic moment of 77.64 μAm^2. After calibration, an empty probe was measured to use later to compensate for the background signal.

Magnetic hysteresis measurements were done in two steps. For the first step, the induced magnetic moment (M) of a specimen was measured as a function of the applied magnetic field (H). The field H cycled between ±1.0 T (with the field increments of 10 mT) depending on the sample characteristics. After the measurement was finished, the empty probe signal was subtracted from the raw data using the AGFM software. The same software was used to remove the diamagnetic and paramagnetic signals to filter out the ferromagnetic signal. The adjusted M(H) curve (called a hysteresis loop) allows to determine three magnetic hysteresis parameters: the saturation magnetization (Ms), saturation remanent magnetization (Mrs), and coercive force (Hc) (Figure 12).

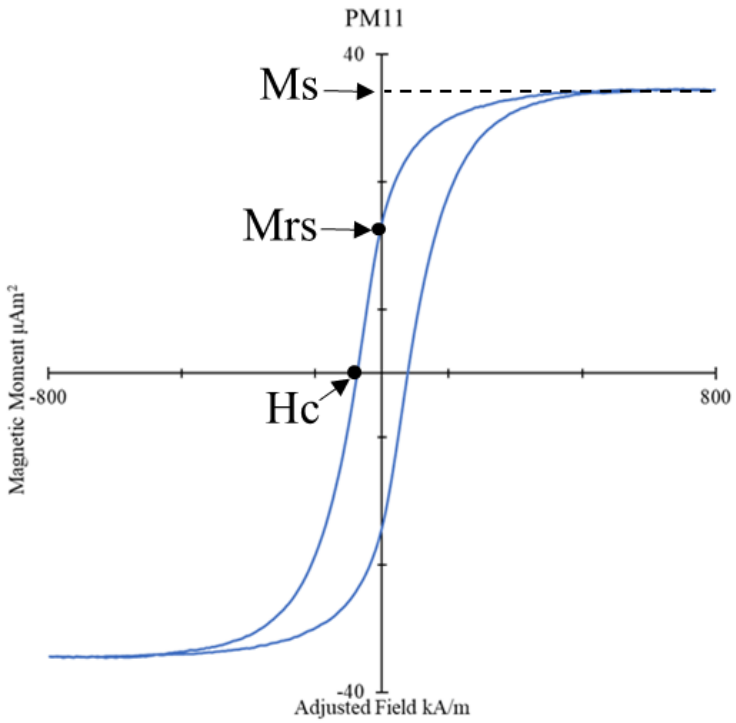

Figure 12. An example of a magnetic hysteresis loop (blue line), M(H), where H is the applied magnetic field, and M is the induced magnetic moment. Ms: Saturation magnetization; Mrs: Saturation remanent magnetization; Hc: Coercive force.

3.0 Results

3.1 Paleomagnetism

Almost all samples from sites representing basaltic flows of Portage Lake Volcanics (PM01-05, PM09-11) manifested a two-component NRM. A low temperature, soft component was removed by temperatures not exceeding 500°C. The characteristic remanent magnetization component (ChRM) was identified by a straight linear demagnetization trajectory toward the origin on a vector endpoint diagram. The ChRM

was typically demagnetized between 530-540°C and 680-690°C (Figure 9). For most samples, paleomagnetic ChRM directions were measured from two specimens per sample. Calculated site-mean directions are shown in Tables 3-13.

PM01				Tilt-corrected	
SAMPLE	Core A	Core P	NRM (emu/cm3)	ChRM Decl	ChRM Incl
B1	4.6	38.0	2.377E-04	312.3	30.7
B2	4.6	38.0	3.606E-04	315.5	19.9
D1	3.4	28.0	1.179E-02	269.7	-45.8
D2	3.4	28.0	1.051E-02	284.8	-49.8
E1	299.5	56.0	6.067E-03	320.5	26.1
E2	299.5	56.0	6.924E-03	323.3	27.9
F1	323.8	65.0	3.082E-03	310.5	26.0
F2	323.8	65.0	3.719E-03	311.7	24.7
G1	59.6	61.0	6.143E-03	315.9	27.9
G2	59.6	61.0	5.407E-03	311.8	26.4
H1	44.3	59.0	6.516E-03	307.8	20.5
I1	44.3	58.0	6.016E-03	314.1	27.0
I2	61.7	58.0	5.274E-03	311.7	23.1
J1	346.9	30.0	3.941E-03	300.6	28.6
K1	351.9	16.0	4.003E-03	311.9	27.8
L1	323.5	20.0	3.442E-03	293.3	28.7
M1	347.2	35.0	4.969E-03	306.6	25.2
M2	347.2	35.0	5.170E-03	306.3	27.0
N1	13.1	5.0	2.963E-03	316.4	26.2
N2	13.1	5.0	2.996E-03	312.8	27.3
O1	6.6	50.0	1.013E-03	294.0	20.9
O2	6.6	50.0	9.483E-04	289.4	19.5
P1	352.9	18.0	8.275E-03	304.2	18.2
Q1	350.7	18.0	6.159E-03	314.4	23.3
Q2	350.7	18.0	5.318E-03	312.9	24.9
R1	352.2	39.0	7.682E-03	306.2	28.1
R2	352.2	39.0	7.339E-03	305.6	29.7
S1	359.3	27.0	1.121E-02	303.5	31.8
S2	359.3	27.0	1.082E-02	302.4	34.0

Table 3. Paleomagnetic results for Site PM01. Core A/Core P: Core azimuth/plunge; NRM: Natural remanent magnetization; ChRM Decl/Incl: Declination and inclination of characteristic remanent magnetization after core orientation and structural attitude corrections.

PM02				Tilt-corrected	
SAMPLE	Core A	Core P	NRM (emu/cm3)	ChRM Decl	ChRM Incl
A1	345.8	60.0	1.598E-04	16.6	6.0
A2	345.8	60.0	1.008E-04	21.6	7.0
B1	28.8	59.5	1.241E-04	N/A	N/A
B2	28.8	59.5	1.192E-04	N/A	N/A
C1	324.2	60.0	1.913E-04	33.0	348.2
C2	324.2	60.0	2.803E-04	31.3	353.5
D1	342.0	61.0	1.683E-04	25.2	350.2
D2	342.0	61.0	1.975E-04	27.6	350.8
E1	333.1	56.0	1.768E-04	25.2	348.0
E2	333.1	56.0	1.593E-04	27.9	347.3
F1	18.4	57.0	2.826E-04	26.9	356.2
G1	3.0	12.5	4.960E-03	32.8	0.7
G2	3.0	12.5	5.431E-03	32.3	358.8

Table 4. Paleomagnetic results for Site PM02. Core A/Core P: Core azimuth/plunge; NRM: Natural remanent magnetization; ChRM Decl/Incl: Declination and inclination of characteristic remanent magnetization after the core orientation and structural attitude corrections.

PM03				Tilt-corrected	
SAMPLE	Core A	Core P	NRM (emu/cm3)	ChRM Decl	ChRM Incl
A1	319.0	45.0	2.539E-04	322.9	36.9
A2	319.0	45.0	2.462E-04	324.3	38.8
B1	315.7	28.0	8.545E-05	327.1	37.8
B2	315.7	28.0	1.030E-04	333.5	38.0
C1	17.9	64.0	3.007E-04	202.1	67.9
C2	17.9	64.0	3.404E-04	191.8	63.1
D1	317.1	45.0	3.637E-04	180.9	55.0
D2	317.1	45.0	3.466E-04	178.3	55.7
E1	14.3	41.0	4.267E-04	322.8	19.0
F1	64.0	52.0	7.913E-04	325.0	13.1
F2	64.0	52.0	8.834E-04	323.9	13.1
G1	321.9	48.0	4.957E-04	340.7	31.0
G2	321.9	48.0	4.156E-04	340.7	33.2
H1	126.6	59.0	2.416E-04	328.3	34.0

Table 5. Paleomagnetic results for Site PM03. Core A/Core P: Core azimuth/plunge; NRM: Natural remanent magnetization; ChRM Decl/Incl: Declination and inclination of characteristic remanent magnetization after the core orientation and structural attitude corrections.

PM04				Tilt-corrected	
SAMPLE	Core A	Core P	NRM (emu/cm3)	ChRM Decl	ChRM Incl
A1	148.7	36.5	3.805E-03	306.5	33.2
A1	148.7	36.5	3.997E-03	308.9	31.4
C1	344.1	35.0	3.736E-03	294.1	17.0
C2	344.1	35.0	3.478E-03	294.3	14.6
D1	314.8	8.0	4.034E-03	297.0	25.3
D2	314.8	8.0	4.304E-03	301.5	26.6
E1	358.9	-8.0	4.965E-03	279.6	24.1
F1	73.9	46.0	4.313E-03	310.2	14.3
F2	73.9	46.0	4.306E-03	311.1	14.9
G1	4.5	32.5	3.564E-03	328.1	29.0
H1	12.2	4.0	2.753E-03	297.0	20.1
I1	7.9	2.0	3.134E-03	293.9	20.4

Table 6. Paleomagnetic results for Site PM04. Core A/Core P: Core azimuth/plunge; NRM: Natural remanent magnetization; ChRM Decl/Incl: Declination and inclination of characteristic remanent magnetization after the core orientation and structural attitude corrections.

PM05				Tilt-corrected	
SAMPLE	Core A	Core P	NRM (emu/cm3)	ChRM Decl	ChRM Incl
A1	293.7	22.0	1.639E-03	300.1	18.1
A2	293.7	22.0	1.731E-03	301.4	17.9
B1	334.4	5.0	1.741E-03	308.1	19.6
D1	31.9	45.0	2.739E-03	317.0	15.8
E1	325.9	25.0	1.287E-03	306.6	23.1
F1	318.4	13.5	5.771E-03	298.0	33.4
G1	1.4	14.0	1.040E-03	302.3	33.5

Table 7. Paleomagnetic results for Site PM05. Core A/Core P: Core azimuth/plunge; NRM: Natural remanent magnetization; ChRM Decl/Incl: Declination and inclination of characteristic remanent magnetization after the core orientation and structural attitude corrections.

PM06				Tilt-corrected	
SAMPLE	Core A	Core P	NRM (emu/cm3)	ChRM Decl	ChRM Incl
A1	212.6	84.0	2.008E-06	287.0	-36.7
C1	164.2	67.5	8.887E-07	150.4	10.1
D1	276.8	52.0	3.153E-06	169.2	-25.6
E1	285.9	72.0	1.640E-06	185.6	32.3
F1	295.6	76.0	2.352E-06	101.4	-70.8

Table 8. Paleomagnetic results for Site PM06. Core A/Core P: Core azimuth/plunge; NRM: Natural remanent magnetization; ChRM Decl/Incl: Declination and inclination of characteristic remanent magnetization after the core orientation and structural attitude corrections.

PM07				Tilt-corrected	
SAMPLE	Core A	Core P	NRM (emu/cm3)	ChRM Decl	ChRM Incl
A1	263.8	44.5	4.067E-05	349.2	5.5
B1	313.8	58.0	4.567E-05	325.8	-10.7
C1	331.0	63.0	9.569E-06	320.8	-43.0
D1	322.0	68.5	7.862E-06	141.8	10.5

Table 9. Paleomagnetic results for Site PM07. Core A/Core P: Core azimuth/plunge; NRM: Natural remanent magnetization; ChRM Decl/Incl: Declination and inclination of characteristic remanent magnetization after the core orientation and structural attitude corrections.

PM08				Tilt-corrected	
SAMPLE	Core A	Core P	NRM (emu/cm3)	ChRM Decl	ChRM Incl
A1	n/a	-10.0	4.058E-06	358.0	59.8

Table 10. Paleomagnetic results for Site PM08. Core A/Core P: Core azimuth/plunge; NRM: Natural remanent magnetization; ChRM Decl/Incl: Declination and inclination of characteristic remanent magnetization after the core orientation and structural attitude corrections.

PM09				Tilt-corrected	
SAMPLE	Core A	Core P	NRM (emu/cm3)	ChRM Decl	ChRM Incl
A1	27.1	41.0	1.842E-04	356.7	27.8
B2	312.1	-6.0	1.064E-04	15.8	5.2
C1	313.6	25.0	9.237E-05	9.2	11.8
D1	350.6	15.0	1.188E-04	355.6	24.0
E1	45.6	8.5	6.717E-04	359.5	32.6
F1	38.5	16.0	8.635E-04	3.5	27.3

Table 11. Paleomagnetic results for Site PM09. Core A/Core P: Core azimuth/plunge; NRM: Natural remanent magnetization; ChRM Decl/Incl: Declination and inclination of characteristic remanent magnetization after the core orientation and structural attitude corrections.

PM10				Tilt-corrected	
SAMPLE	Core A	Core P	NRM (emu/cm3)	ChRM Decl	ChRM Incl
A1	276.5	29.0	2.355E-04	319.0	30.3
B1	273.7	23.0	2.235E-04	320.5	29.8
C1	280.2	25.5	2.566E-04	299.5	35.8
E1	287.4	32.0	3.837E-04	309.0	34.6
F1	327.8	82.5	3.967E-04	163.1	82.0
G1	340.6	21.0	4.169E-04	307.3	27.1

Table 12. Paleomagnetic results for Site PM10. Core A/Core P: Core azimuth/plunge; NRM: Natural remanent magnetization; ChRM Decl/Incl: Declination and inclination of characteristic remanent magnetization after the core orientation and structural attitude corrections.

PM11				Tilt-corrected	
SAMPLE	Core A	Core P	NRM (emu/cm3)	ChRM Decl	ChRM Incl
A1	176.5	75.0	2.355E-04	336.5	71.2
B1	147.8	61.5	2.235E-04	310.8	43.6
C1	298.5	37.5	2.566E-04	309.2	58.9
E1	151.5	80.5	3.837E-04	341.6	37.9
F1	112.7	60.5	3.967E-04	311.4	64.1

Table 13. Paleomagnetic results for Site PM11. Core A/Core P: Core azimuth/plunge; NRM: Natural remanent magnetization; ChRM Decl/Incl: Declination and inclination of characteristic remanent magnetization after the core orientation and structural attitude corrections.

Site PM01 samples (N=27) yielded well-grouped ChRM directions except for sample PM01D, which was excluded from the site-mean calculation (Figure 13). ChRM directions for site PM02 are all well-grouped although sample PM02A showed more northerly directions (Figure 14). Nevertheless, all PM02 directions (N=11) were used to calculate the site-mean. Most ChRM directions from site PM03 samples have consistently very shallow inclination and NNW declination. However, ChRM directions from samples PM03C and PM03D are very different, with an inclination of ~60° and westerly declination (Figure 15). Potentially, these samples were collected from a block that was not in situ and, therefore, they were excluded from the site-mean calculation. Samples from sites PM04 (N=12), PM05 (N=7), PM09 (N=6), PM10 (N=5), and PM11 (N=5) yielded well-grouped directions within each site (Figures 16-20).

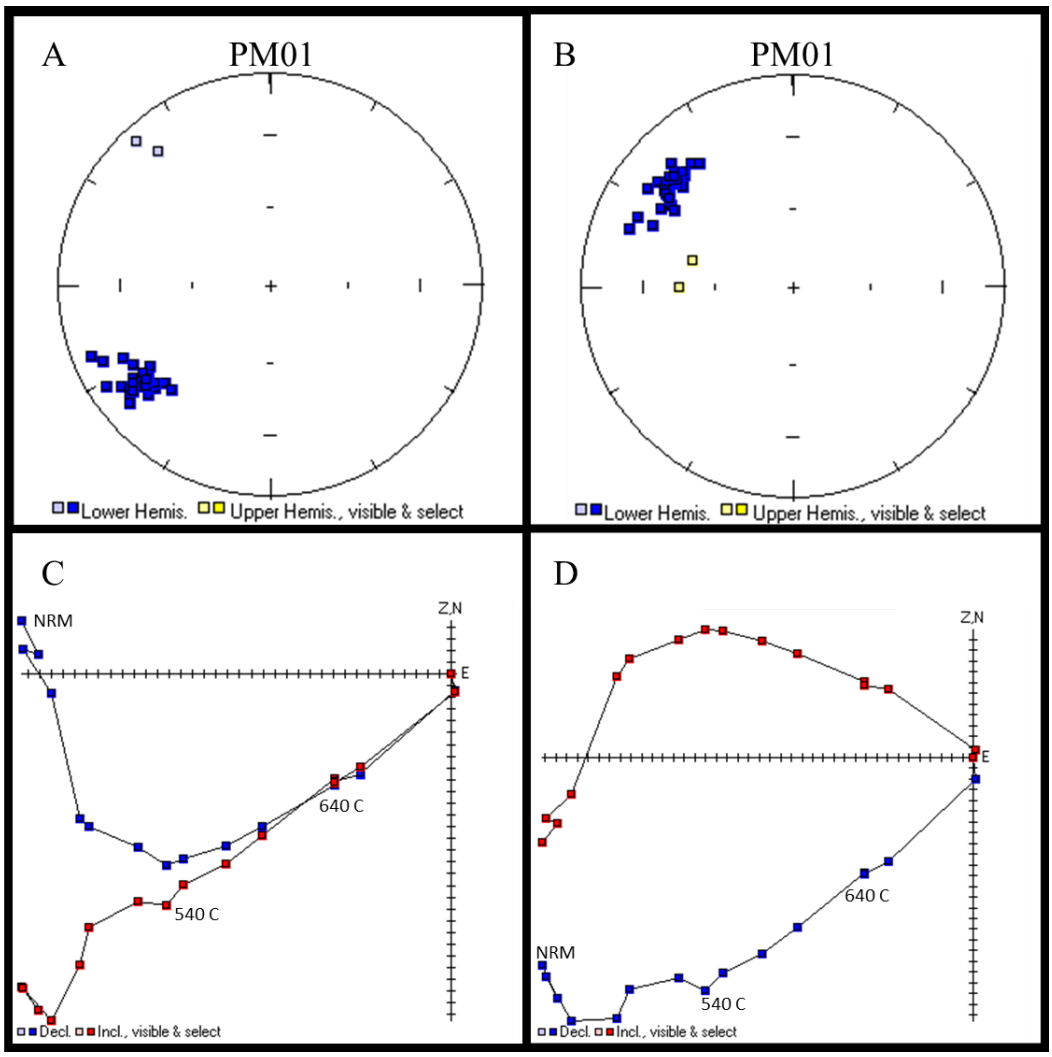

Figure 13. Equal-area plot of paleomagnetic characteristic directions for Site PM01 in the core (A) and geographic (B) coordinates (see text). Highlighted data points were used to calculate the site-mean direction. (C, D). Representative vector end-point diagram showing thermal demagnetization before (C) and after (D) correction for core and structural orientation. The numbers show temperatures of selected temperature steps.

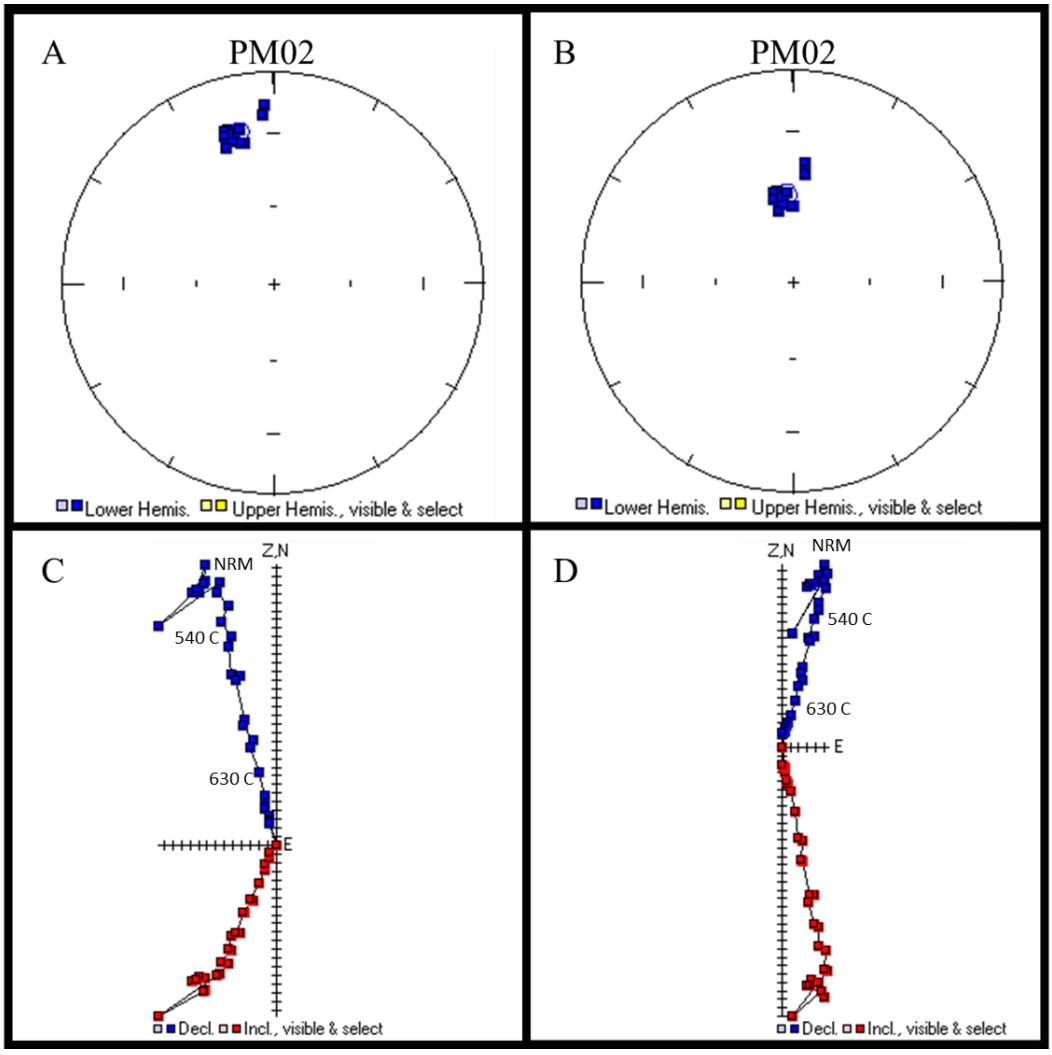

Figure 14. Equal-area plot of paleomagnetic characteristic directions for Site PM02 in the core (A) and geographic (B) coordinates (see text). Highlighted data points were used to calculate the site-mean direction. (C, D). Representative vector end-point diagram showing thermal demagnetization before (C) and after (D) correction for core and structural orientation. The numbers show temperatures of selected temperature steps.

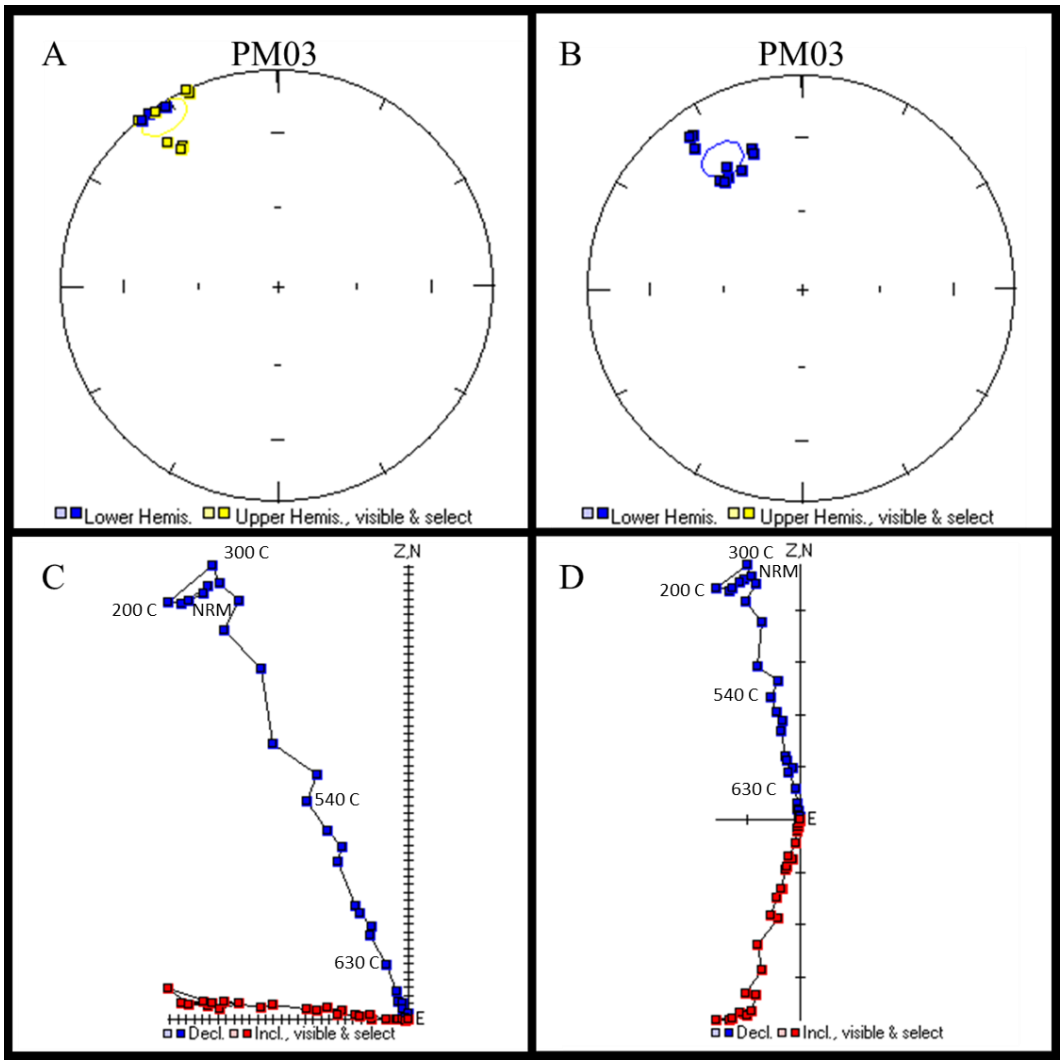

Figure 15. Equal-area plot of paleomagnetic characteristic directions for Site PM03 in the core (A) and geographic (B) coordinates (see text). Highlighted data points were used to calculate the site-mean direction. (C, D). Representative vector end-point diagram showing thermal demagnetization before (C) and after (D) correction for core and structural orientation. The numbers show temperatures of selected temperature steps.

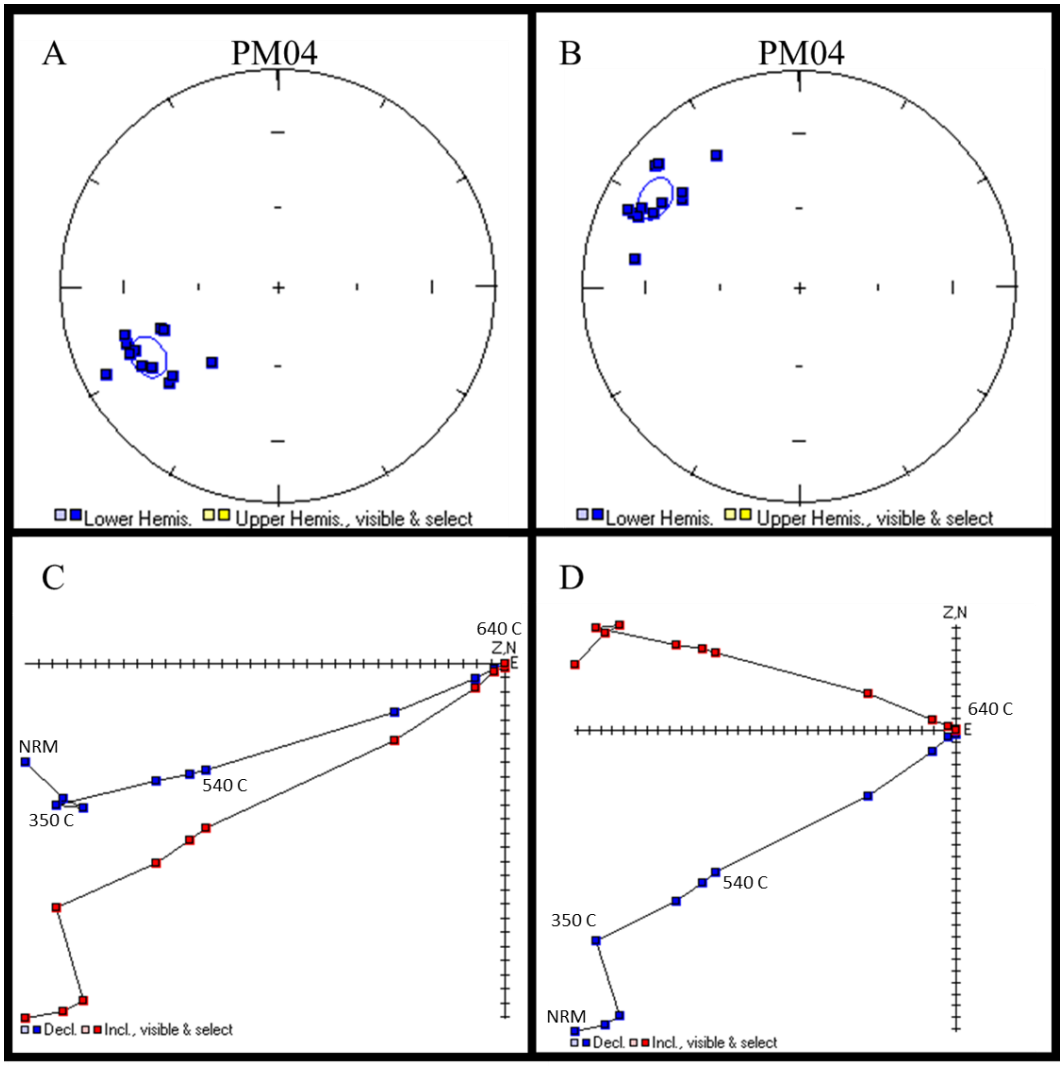

Figure 16. Equal-area plot of paleomagnetic characteristic directions for Site PM04 in the core (A) and geographic (B) coordinates (see text). Highlighted data points were used to calculate the site-mean direction. (C, D). Representative vector end-point diagram showing thermal demagnetization before (C) and after (D) correction for core and structural orientation. The numbers show temperatures of selected temperature steps.

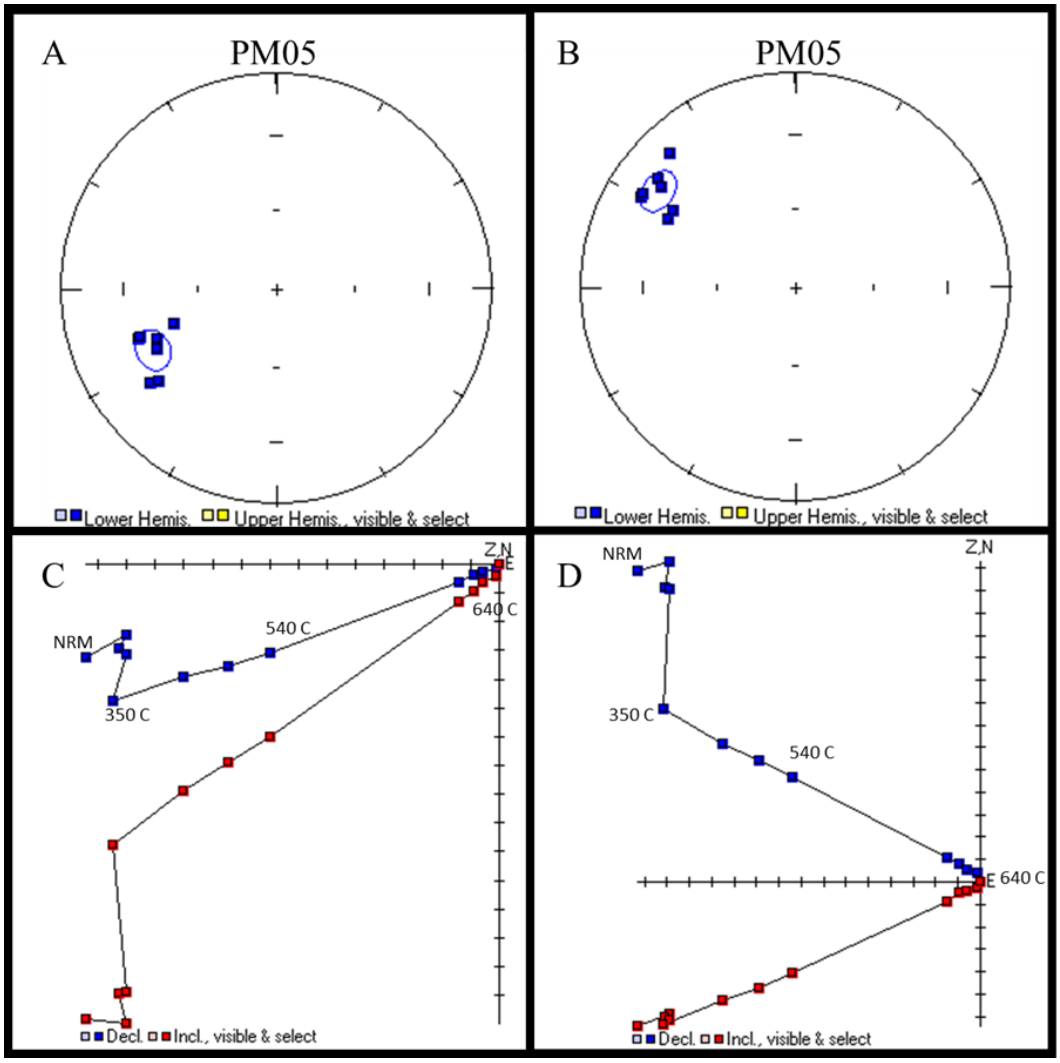

Figure 17. Equal-area plot of paleomagnetic characteristic directions for Site PM05 in the core (A) and geographic (B) coordinates (see text). Highlighted data points were used to calculate the site-mean direction. (C, D). Representative vector end-point diagram showing thermal demagnetization before (C) and after (D) correction for core and structural orientation. The numbers show temperatures of selected temperature steps.

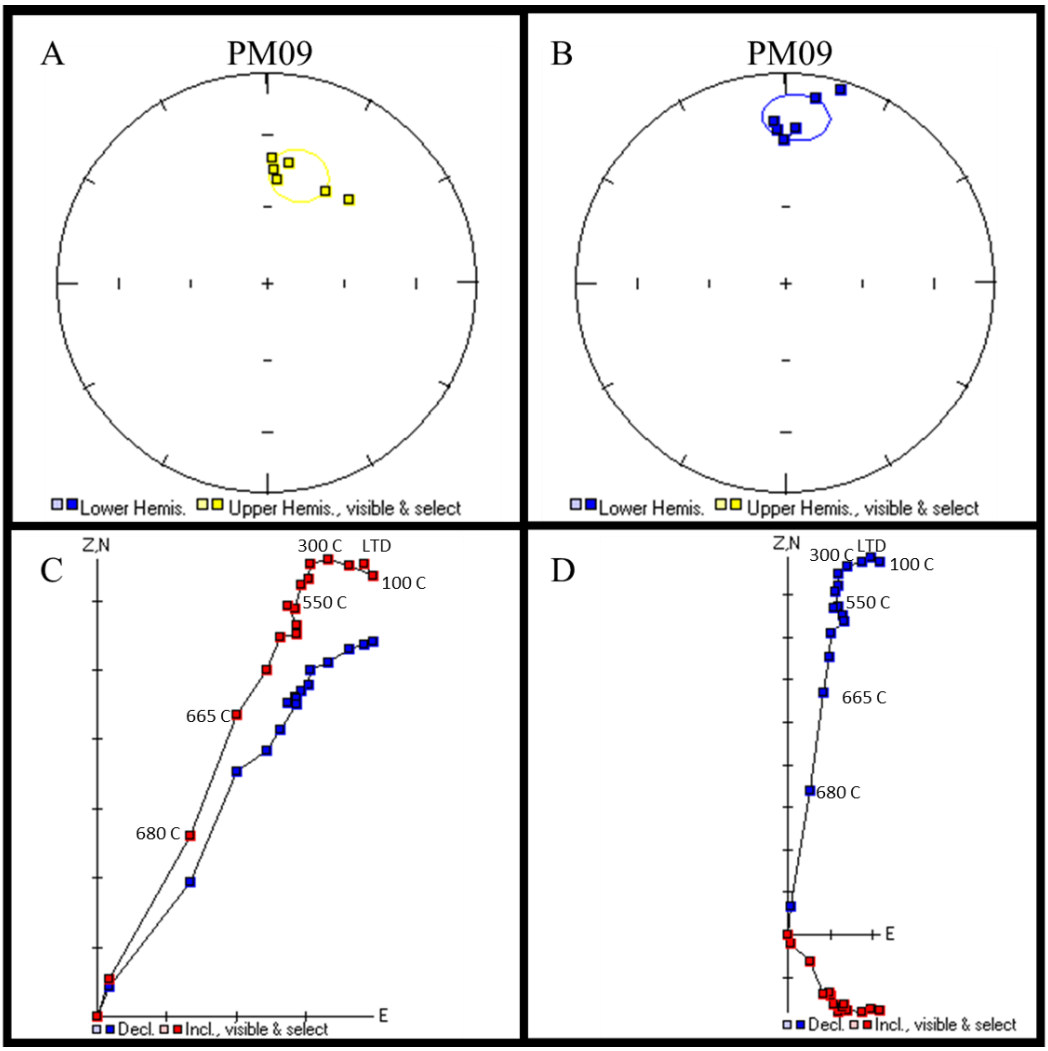

Figure 18. Equal-area plot of paleomagnetic characteristic directions for Site PM09 in the core (A) and geographic (B) coordinates (see text). Highlighted data points were used to calculate the site-mean direction. (C, D). Representative vector end-point diagram showing thermal demagnetization before (C) and after (D) correction for core and structural orientation. The numbers show temperatures of selected temperature steps.

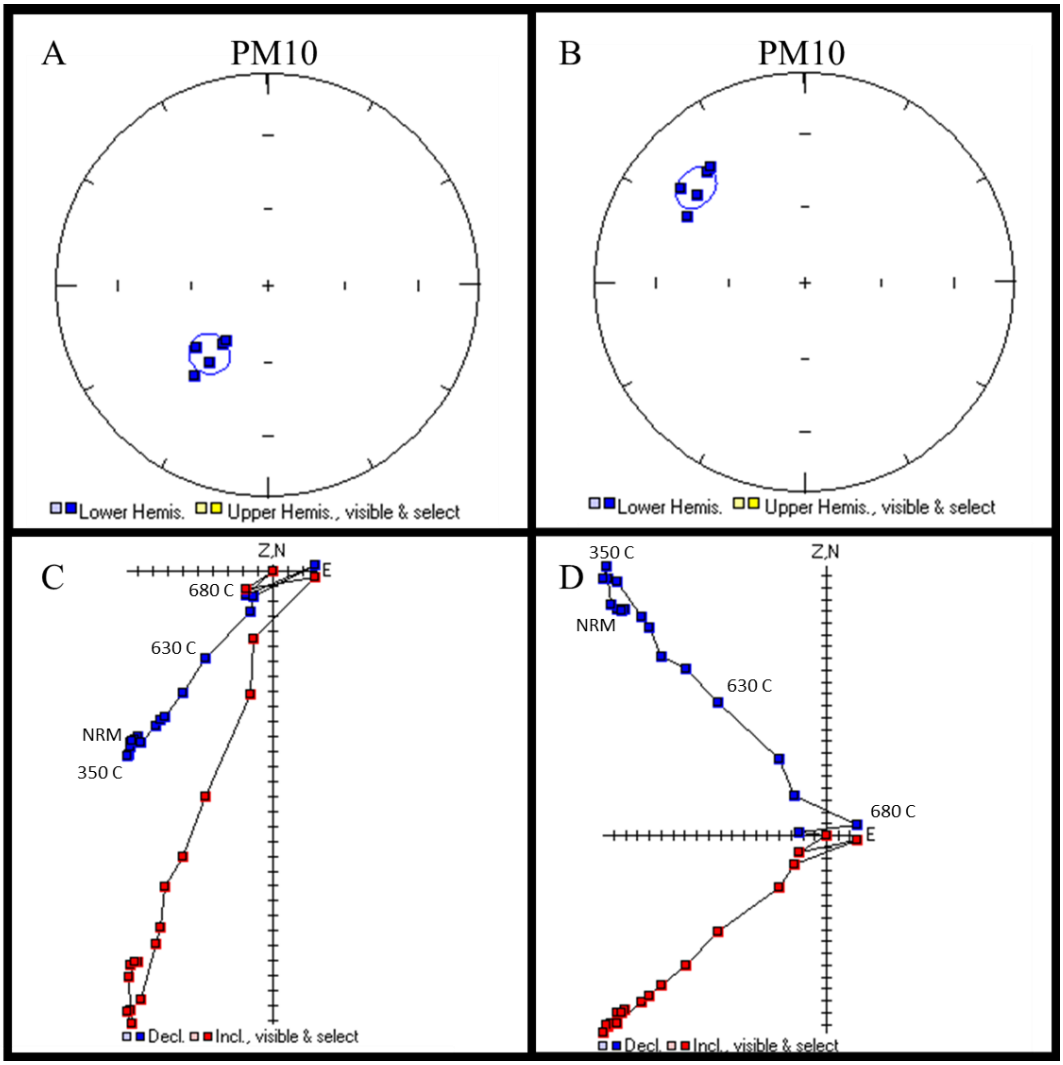

Figure 19. Equal-area plot of paleomagnetic characteristic directions for Site PM10 in the core (A) and geographic (B) coordinates (see text). Highlighted data points were used to calculate the site-mean direction. (C, D). Representative vector end-point diagram showing thermal demagnetization before (C) and after (D) correction for core and structural orientation. The numbers show temperatures of selected temperature steps.

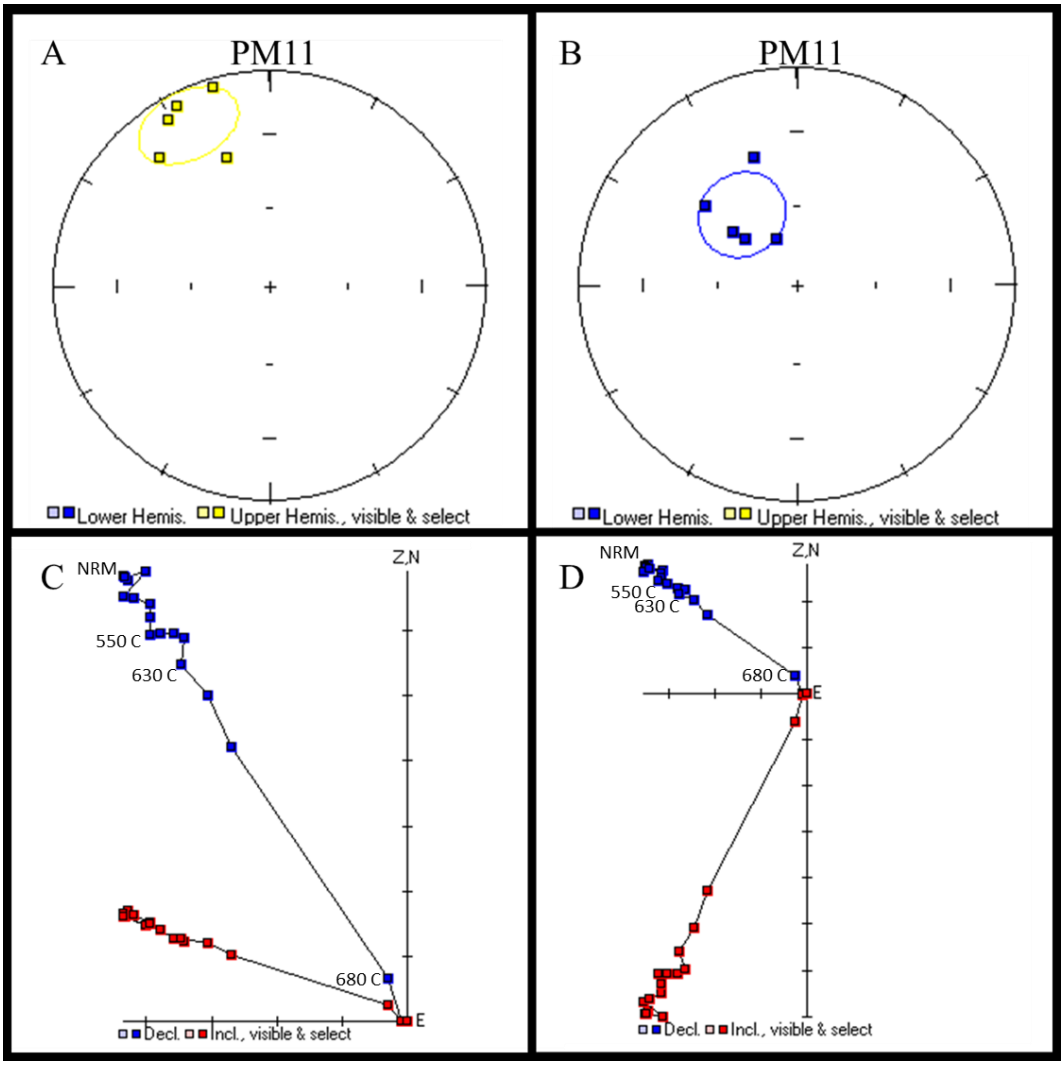

Figure 20. Equal-area plot of paleomagnetic characteristic directions for Site PM11 in the core (A) and geographic (B) coordinates (see text). Highlighted data points were used to calculate the site-mean direction. (C, D). Representative vector end-point diagram showing thermal demagnetization before (C) and after (D) correction for core and structural orientation. The numbers show temperatures of selected temperature steps.

After core and structural orientation corrections were applied, site-mean directions for Sites PM01, PM03, PM04, PM05, PM10, and PM11 had northeasterly declinations ranging from 300° to 330° and shallow-to-intermediate inclinations ranging from 23° to 32°. These directions are similar to group-mean directions published for the Portage Lake Volcanics in prior studies (Table 1). However, corrected site-mean directions for Sites PM02 and PM09 have northerly declinations and shallow (PM09) to intermediate (PM02) inclinations (Table 2; Figures 14b,18b). This is unlikely to result from a recent viscous magnetization overprint because uncorrected values for Site PM09 have negative inclinations (i.e., opposite to the recent field direction), and ChRM directions for both sites are based on the magnetically hard portion of the unblocking temperature spectra.

Five of six measured samples from Site PM06 yielded noisy but still interpretable thermal demagnetization vector plots (Figure 21b). The ChRM component was defined over the 550-700°C range and is primarily carried by hematite. However, ChRM directions are scattered over the equal-area plot (Figure 21a); therefore, no site-mean direction was calculated. Samples from Site PM07 showed a two-component NRM with a well-defined ChRM defined over the 550-700°C range (Figure 22). Similar to Site PM06, a substantial portion of the ChRM is carried by hematite. A single sample from Site PM08 yielded a two-component NRM with most of the ChRM demagnetized within the 100-350°C temperature range (Figure 23). The direction of this ChRM is close to the present field direction in the area so that it was interpreted as a viscous overprint by the recent geomagnetic field.

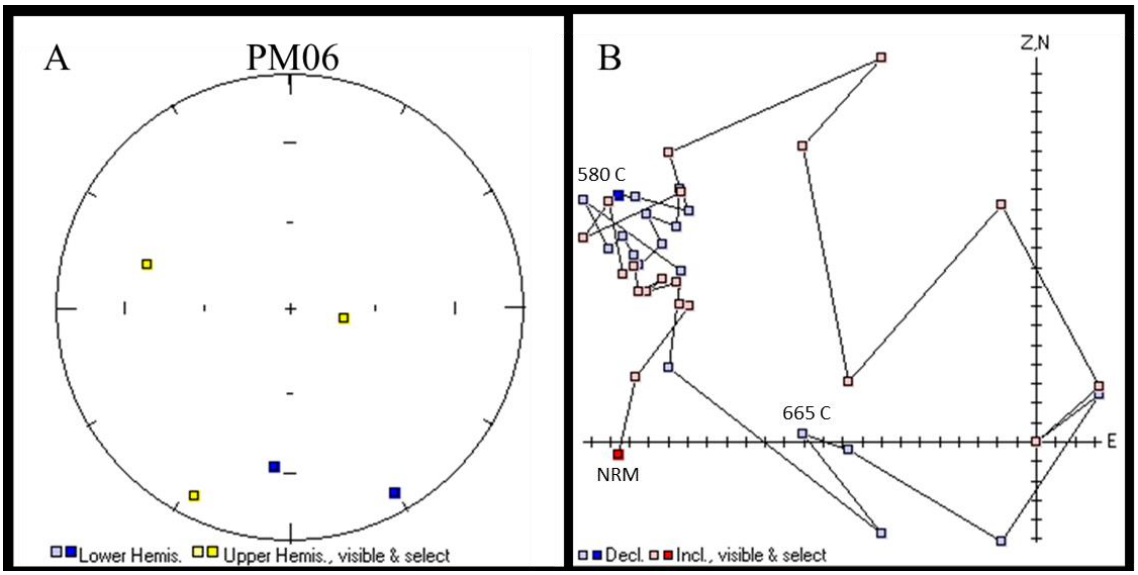

Figure 21. Equal-area plot of paleomagnetic characteristic directions for Site PM06 (A) and a typical vector end-point plot (B) (see text).

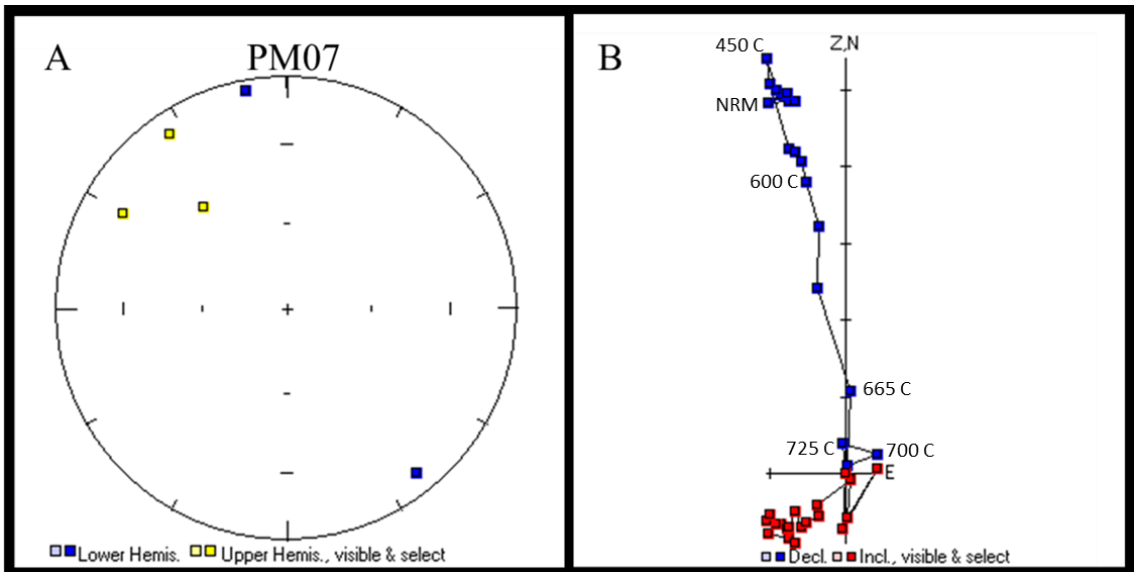

Figure 22. Equal-area plot of paleomagnetic characteristic directions for Site PM07 (A) and a typical vector end-point plot (B) (see text).

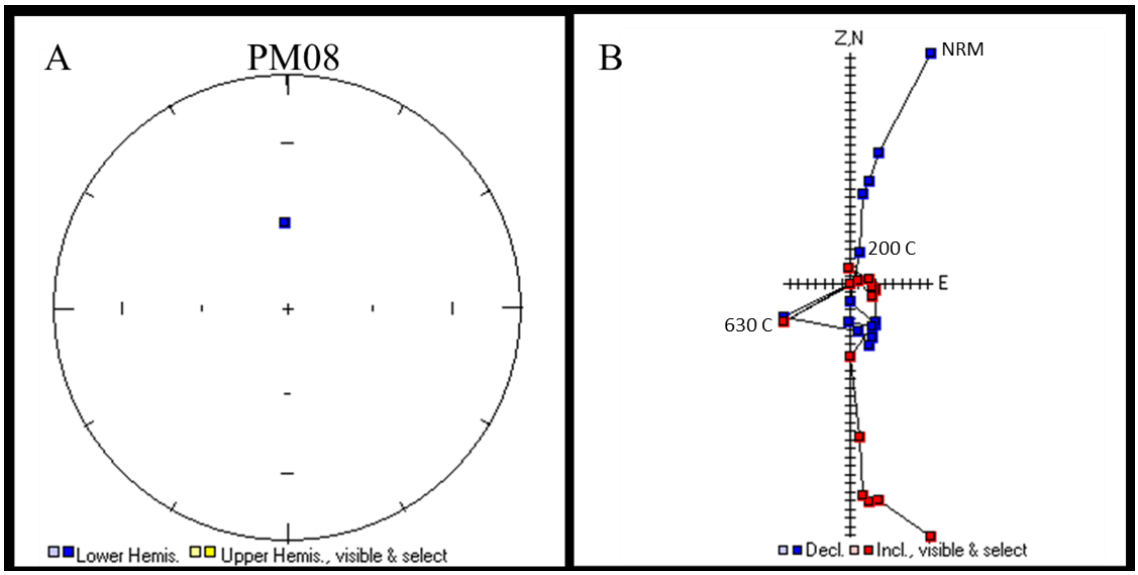

Figure 23. Equal-area plot of paleomagnetic characteristic direction for Site PM09 (A) and the corresponding vector end-point plot (B) (see text).

3.2 Thermomagnetic Analyses

For all sites representing basaltic flows (PM01-05, PM09-11), low-field magnetic susceptibility versus temperature curves revealed the presence of a magnetic phase with Curie temperatures in a range of 570 °C to 585 °C, indicating magnetite to low-Ti titanomagnetite as a magnetic carrier (Figure 25,26). The thermomagnetic curves were non-reversible for all sites except PM04, which exhibited nearly-reversible behavior. For all eight sites, an increase of room-temperature magnetic susceptibility, after the high-temperature step, was observed. This increase varied from approximately 9% for site PM04 to 1240% for site PM10.

The presence of a characteristic peak at approximately -153 °C, associated with the Verwey transition (Verwey, 1939), confirms the presence of nearly-stoichiometric

magnetite in the samples of sites PM04 and PM05. Much smaller inflections of the first low-temperature curves at about the same temperature, -153 °C, suggest that some magnetite is also in samples from sites PM03, PM09, PM10. However, the principal magnetic carrier at these sites and sites PM01, PM02, and PM11 is likely low-Ti titanomagnetite, which does not undergo phase transitions at cryogenic temperatures.

In addition, high-temperature thermomagnetic curves for all sites except PM05, indicate the presence of another ferromagnetic phase with a Curie temperature up to 700 °C (notably in PM03 and PM11) (Figure 24,25). This mineral phase was interpreted as hematite. Although presence of hematite is not always well-expressed on low-field thermomagnetic curves, this high-temperature observation is consistent with NRM demagnetization curves that clearly show an NRM component carried by a magnetic mineral with Curie temperatures above 650 °C. The thermomagnetic curves between 600°C and 700°C are irreversible, indicating that hematite is transformed into another phase by heating.

All PLV sites exhibit a noticeable Verwey transition on the second low-temperature run curves, which indicates neoformation of magnetite by heating during the high-temperature run. The most likely mechanisms for this are reduction of hematite to magnetite and heating-induced magnetic transformation of clays (e.g., Hirt et al., 1993; Kosterov and Prévot, 1998; Tarduno and Smirnov, 2004).

Interestingly, sites PM01, PM04, and PM05 from structural domain A (north-dipping lava flows) exhibit similar behavior during heating. Their thermomagnetic curves

exhibit an increase in magnetic susceptibility upon heating from 200 to 500°C, indicating the presence of titanomagnetite with varying amounts of titanium. Upon cooling, the increased magnetic susceptibility disappears, which, along with the greater peak of the Verwey transition on the post-heating low-temperature run, suggests temperature-induced unmixing of homogeneous titanomagnetite into Ti oxide and low-Ti magnetite phases (e.g., Smirnov et al., 2005). The similarity in this behavior is greatest for sites PM04 and PM05, which may indicate that they sample the same basaltic flow. Site PM01 may belong to the same flow or to a co-genetic flow erupted shortly before or after. In contrast, Site PM10 (structural domain B) from a north-dipping flow exhibited a very different thermomagnetic behavior and, therefore, is likely to belong to a different lava flow.

Sites PM02 and PM03 from structural domain D (southeast-dipping lava flows) exhibit different thermomagnetic behavior and thus are likely to belong to two different flows. The more expressed Hopkinson peak, approximately 585 °C, for site PM03 may indicate presence of finer magnetic grains that are closer to a single-domain state.

Sites PM09 and PM11 from structural domain C (south-dipping lava flows) are characterized by very similar thermomagnetic behavior, indicating that they represent the same lava flow or co-genetic lava flows. They are certainly different from the flows at sites PM02 and PM03.

Overall, thermomagnetic results from the PLV sites are consistent with the results reported by prior investigations of the Portage Lake Volcanics.

A sample from site PM06 (brecciated sandstone) shows irreversible thermomagnetic behavior (Figure 26A). The initial low-temperature run and the heating leg suggest presence of low-Ti titanomagnetite together with a substantial amount of hematite, which converts into fine-grained magnetite upon the temperature treatment. A sample from site PM07 (brecciated basalt) shows thermomagnetic behavior similar to that of sites PM04 and PM05 (Figure 26B). Magnetite seems to be the dominant magnetic mineral, with some titanomagnetite indicated by a bump on the heating curve between 200 and 450°C. No thermomagnetic analyses were performed on the single sample of site PM08 (clastic dike).

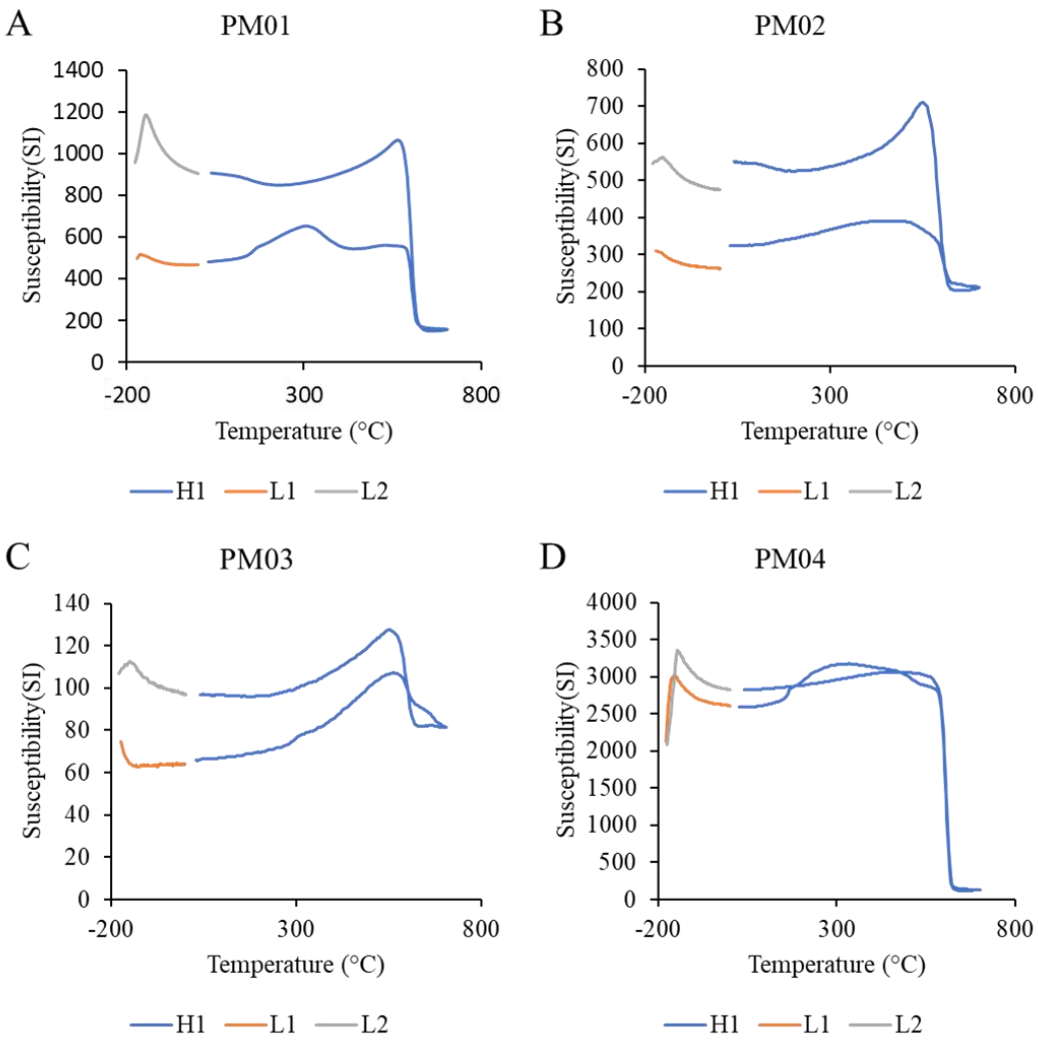

Figure 24. Temperature dependency of low-field magnetic susceptibility for sites representing lava flows of the PLV: PM01 (A), PM02 (B), PM03 (C), and PM04 (D). L1 and L2 denote the first and second low-temperature runs (see text).

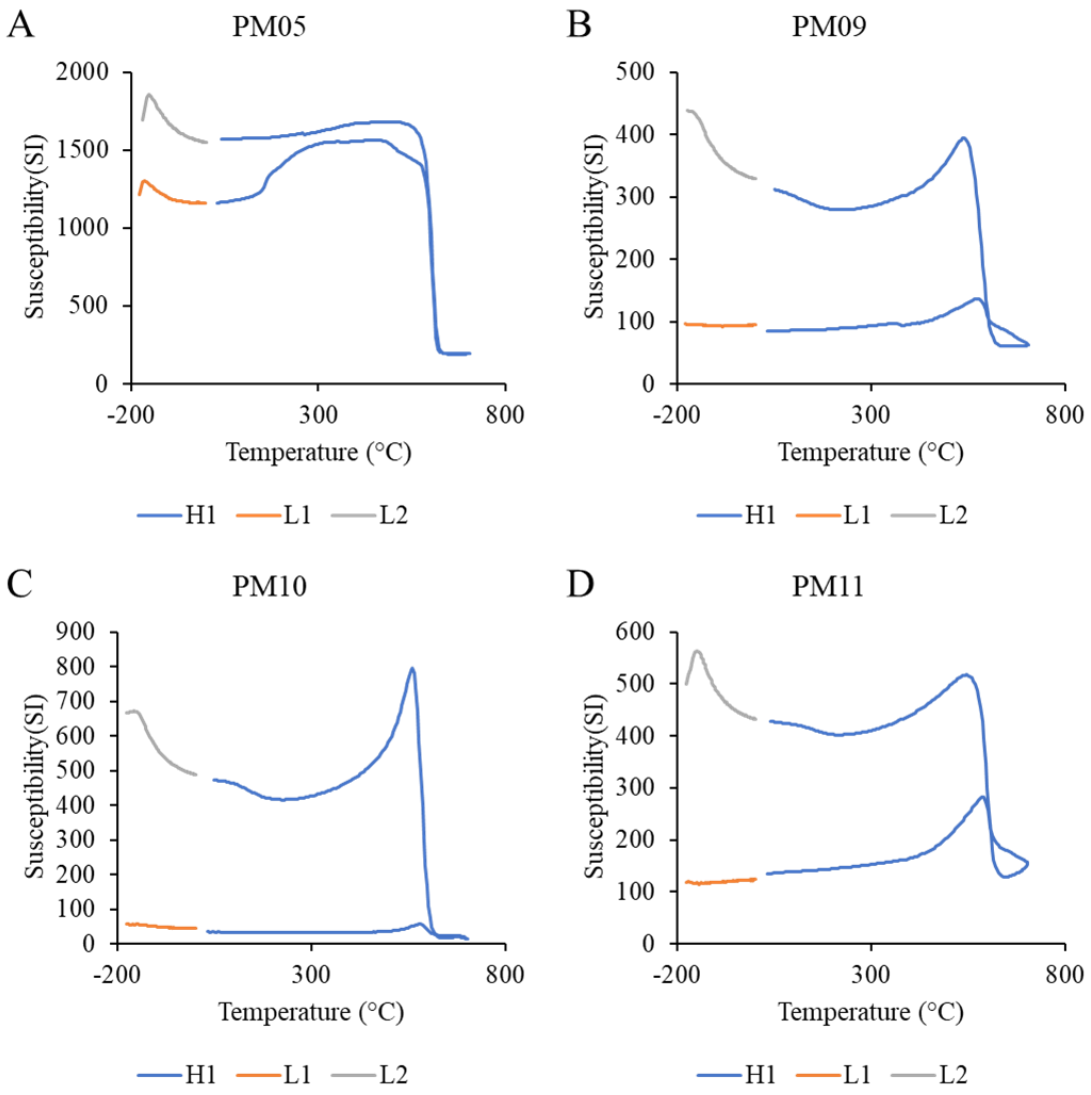

Figure 25. Temperature dependency of low-field magnetic susceptibility for sites representing lava flows of the PLV: PM05 (A), PM09 (B), PM10 (C), and PM11 (D). L1 and L2 denote the first and second low-temperature runs (see text).

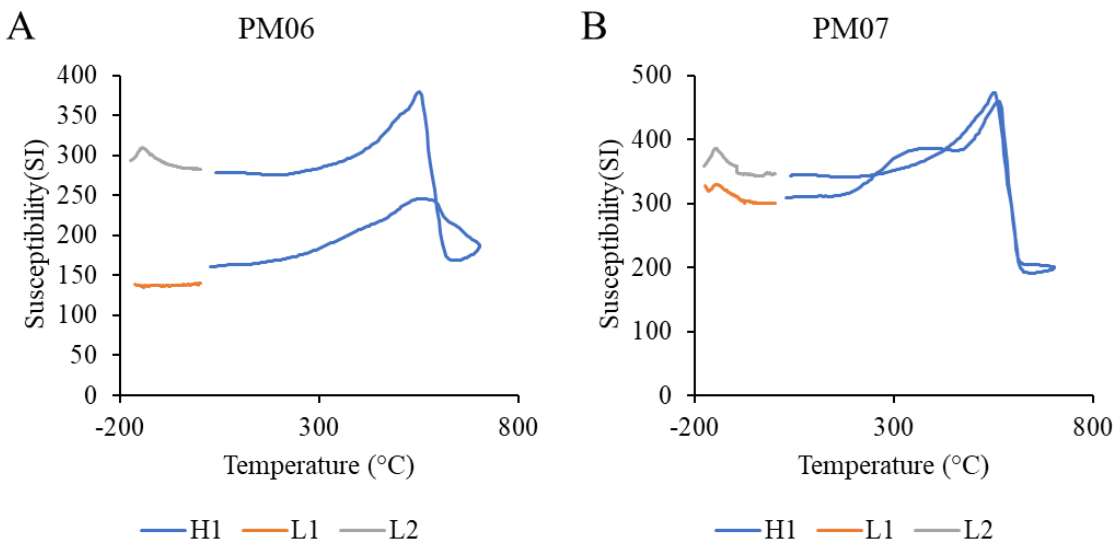

Figure 26. Temperature dependency of low-field magnetic susceptibility for sites PM06 (A) and PM07 (B). L1 and L2 denote the first and second low-temperature runs (see text).

3.3 Magnetic Hysteresis Analyses

Hysteresis measurements suggest a pseudo-single domain (PSD) magnetic carrier in all samples (Figure 27,28,31). Relatively high coercivities for samples from some flows suggest the presence of hematite (Figure 29,30). Wasp-waisted hysteresis loops of some samples (PM03, PM06, and PM07) indicate the presence of magnetic phases with different coercivities such as magnetite and hematite (Tauxe et al., 1996).

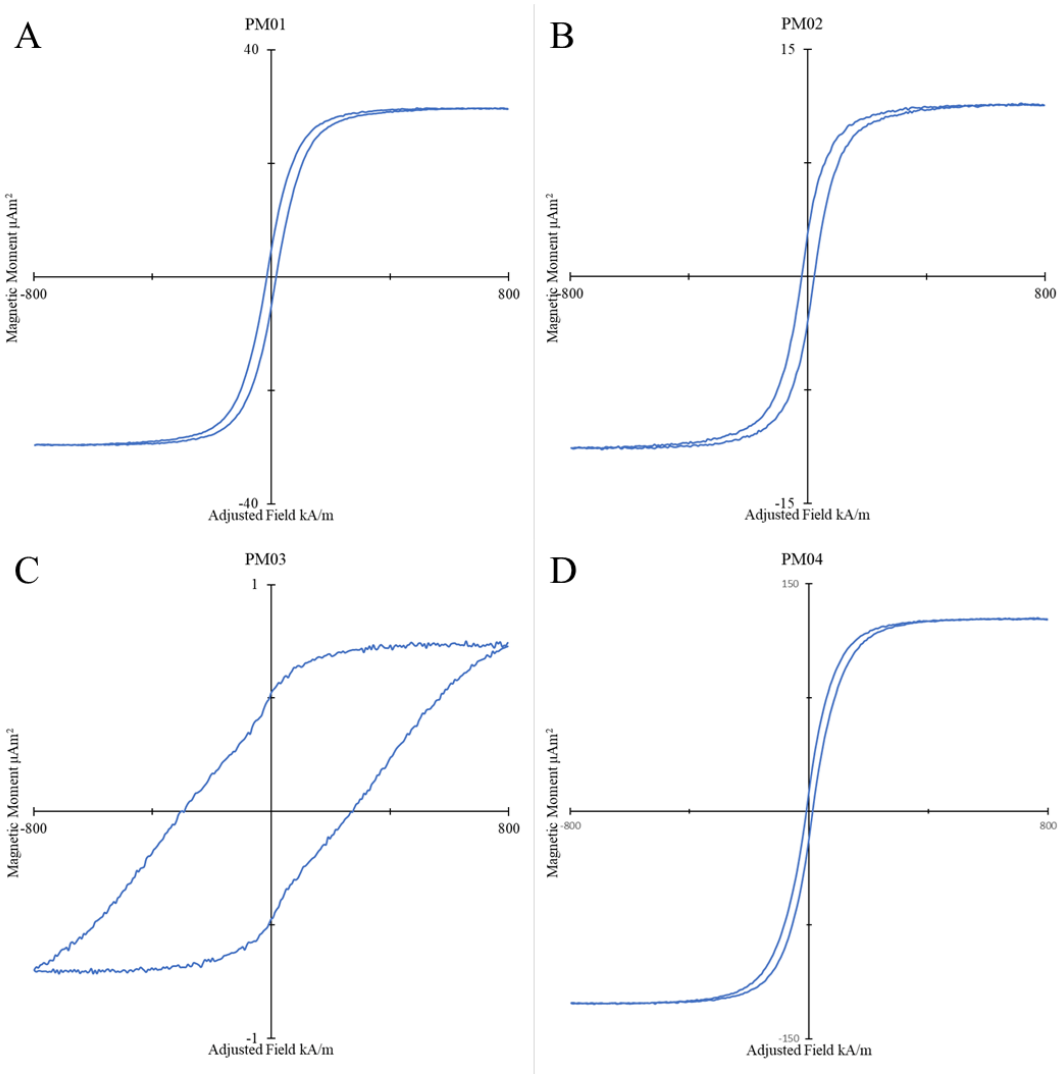

Figure 27. Magnetic hysteresis loops (after paramagnetic slope correction) measured from sites representing lava flows of the PLV PM01 (A), PM02 (B), PM03 9C), and PM04 (D).

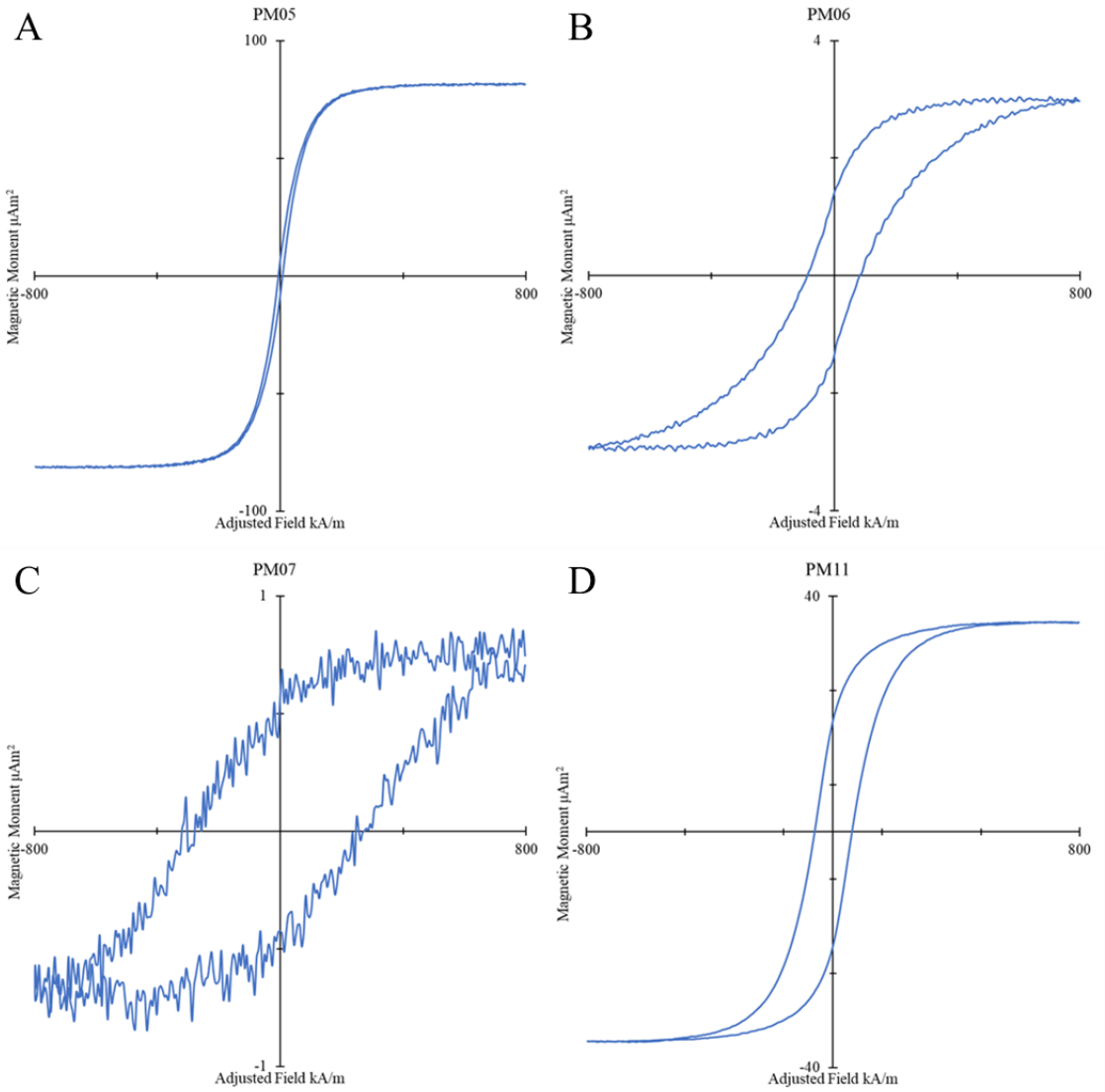

Figure 28. Magnetic hysteresis loops (after paramagnetic slope correction) measured from sites PM05 (A) and PM11 (D) representing lava flows of the PLV, and sites PM06 (B) and PM07 (C) representing fault breccia along a segment of the Keweenaw Fault system.

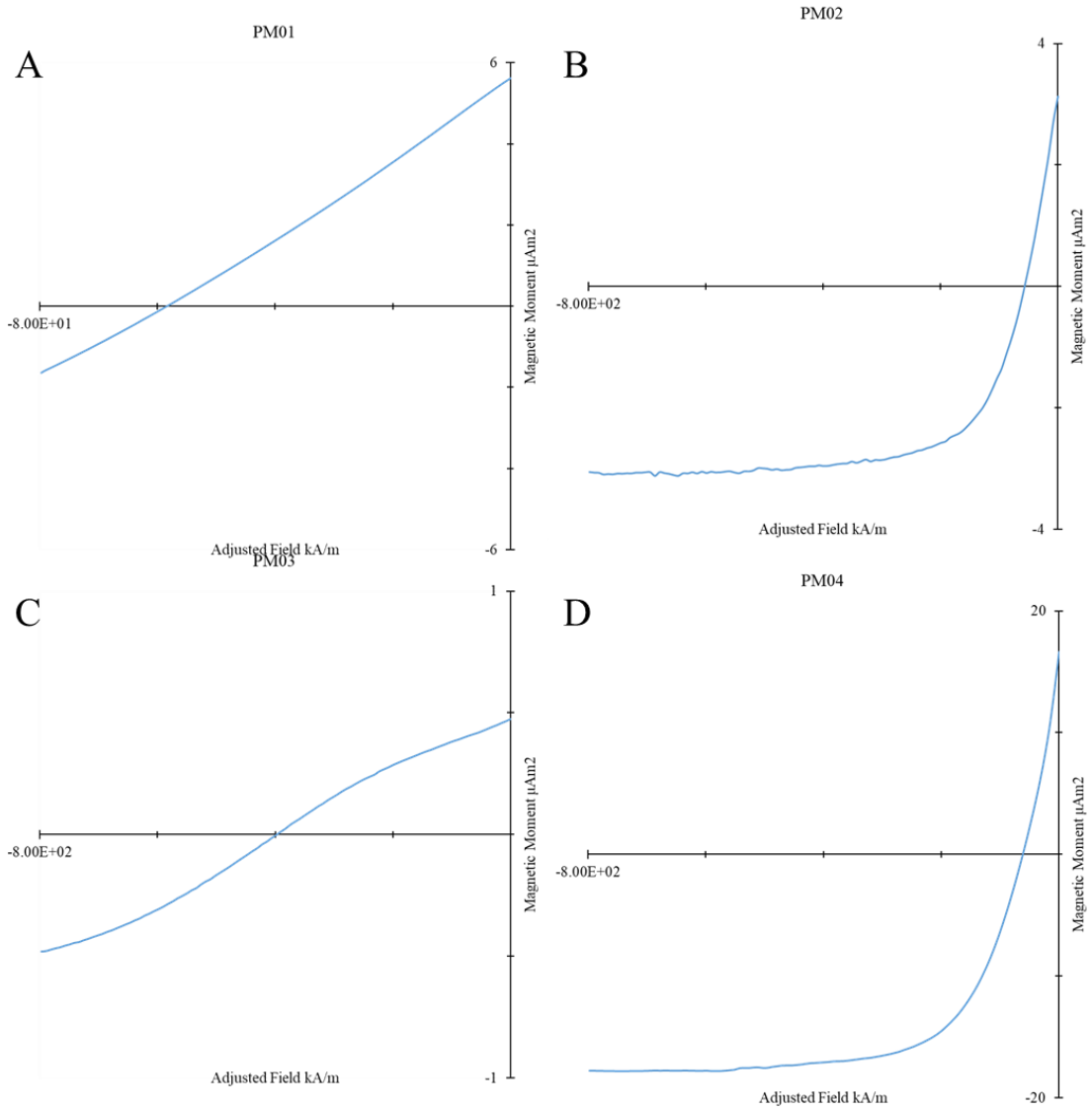

Figure 29. Backfield demagnetization curves for sites PM01-PM04. Non-saturated curves A and C indicate presence of hematite.

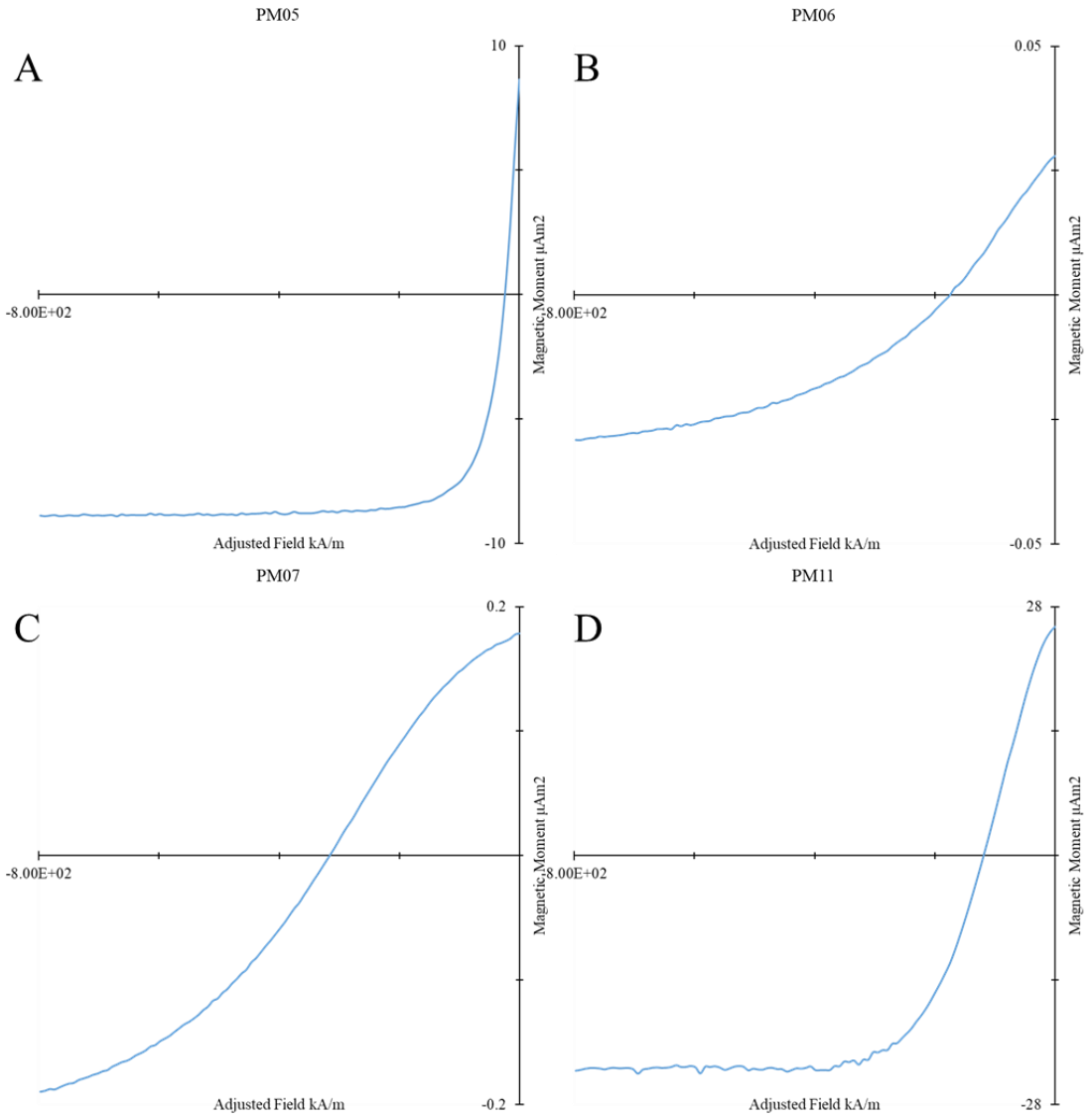

Figure 30. Backfield demagnetization curves for sites PM05-PM07 and PM11. Non-saturated curves B and C indicate presence of hematite.

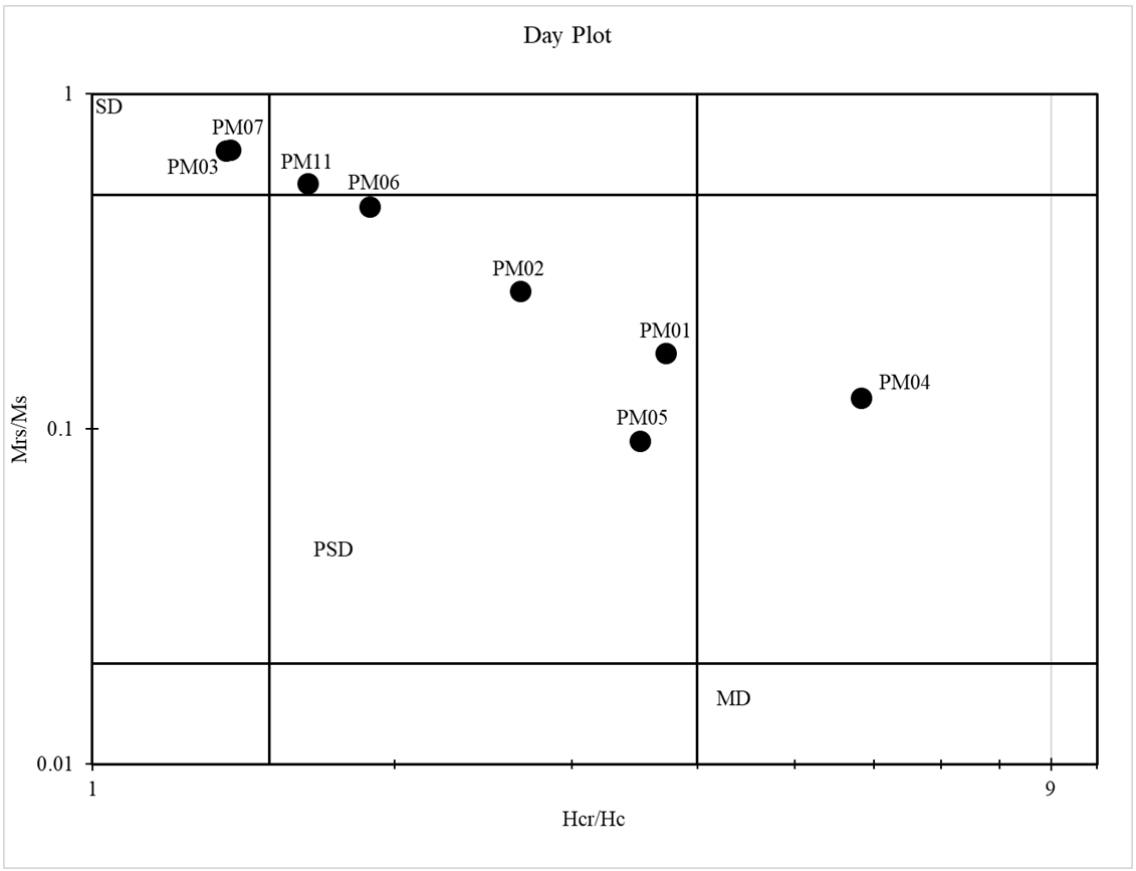

Figure 31. The Day plot showing hysteresis data for sites PM01-PM07 and PM11. The data suggests that magnetic carriers within the samples are mainly single-domain or pseudo-single-domain. SD single-domain, PSD pseudo-single-domain, and MD multi-domain.

4.0 Discussion

Thermomagnetic analyses of the PLV basaltic flows (Sites PM01-PM05 and PM09-PM11) indicate that their principal magnetic carriers are magnetite, titanomagnetite, and hematite. These minerals are identified by their Curie temperatures as well as by the presence of the Verwey transition at -153°C in some samples. Hematite

likely formed during rift inversion as a result of hydrothermal fluid activity (e.g., Browning and Beske-Diehl, 1987). Observed irreversibility of the thermomagnetic curves indicates that the lava flows have not experienced major re-heating since the termination of rifting. This conclusion is further supported by the irreversibility of the thermomagnetic curves for Sites PM06-08. Magnetic hysteresis analyses reveal pseudo-single domain (PSD) characteristics for all samples, which implies that they are able to retain a paleomagnetic signal for billions of years. This result provides additional confidence in the primary nature of the paleomagnetic signal recorded by the flows. Overall, these rock-magnetic results are consistent with the findings reported for PLV lava flows in prior studies (e.g., Browning and Beske-Diehl, 1987; Li and Beske-Diehl, 1993; Hnat et al., 2006; Michels, 2013; Kulakov, 2014).

Based on similar characteristic features of thermomagnetic curves, Sites PM01, PM04, PM05 probably represent the same lava flow or two co-genetic flows. This interpretation is corroborated by the similarity of site-mean paleomagnetic directions from Sites PM01, PM04, and PM05 (Table 14; Figure 32). The similarly north-dipping flow sampled at Site 10 is most likely not related to flows at these sites. Sites PM09 and PM11 may represent one, or two co-genetic flows. Sites PM02 and PM03 likely belong to two unrelated lava flows. While these interpretations are somewhat tentative, the use of rock magnetic characteristics to fingerprint individual lava flows represents a promising direction for future work.

All eight sites that sampled PLV basaltic flows yielded reliable ChRM directions generally defined within the ~540°C-700°C unblocking temperature range (Figures 13-

20). In PLV rocks, remanence carried by hematite (unblocked above 600°C) has been considered to be a secondary component formed by hydrothermal activity during post-rift compression, and remanence carried by magnetite (unblocked within ~540°C-590°C) has been considered to be the primary component acquired during initial cooling of lava flows (e.g., Browning and Beske-Diehl, 1987). However, the difference between these two directions is very small and, even if present, would not be relevant for the purposes of this project. Data obtained in this study show no difference in paleomagnetic direction carried by titanomagnetite/magnetite and hematite in the same sample.

SITE	Geogr. D (°)	Geogr. I (°)	Tilt D (°)	Tilt I (°)	a95 (°)	N/n
PM-01	233.8	23.8	308.7	26.2	2.8	0.70
PM-02	346.7	27.4	355.7	55.9	4.1	0.64
PM-03	326.2	-6.5	328.8	29.7	7.2	0.80
PM-04	241.4	32.9	301.7	23	7	0.75
PM-05	243.6	36.2	305	23.2	7.1	1
PM-06	N/A	N/A	N/A	N/A	N/A	N/A
PM-07	N/A	N/A	N/A	N/A	N/A	N/A
PM-08	N/A	N/A	N/A	N/A	N/A	N/A
PM-09	16.3	-45.6	3.7	21.6	10.8	1.0
PM-10	220.5	55	311.2	31.8	7.8	1.4
PM-11	333.3	-16.8	322.2	56	16.1	1.2

Table 14. Structurally corrected paleomagnetic directions of sites PM01-PM11. Geogr. D and I represent the paleomagnetic direction for sites, Tilt D and Tilt I represent the tilt-corrected paleomagnetic direction for sites, α95 is the 95% confidence circle around the site-mean direction, and N is the number of samples used for site mean direction.

After applying the structural correction for bedding orientation, paleomagnetic directions from Sites PM01, PM03, PM04, PM05, PM10, and PM11 plot close to the

group-mean paleomagnetic direction reported for the PLV by Kulakov (2014) and Browning and Beske-Diehl (1987) (Table 14; Figure 32). These results constitute a positive fold test (Butler, 1992) and thus support the hypothesis of fault-induced folding of the PLV in the area.

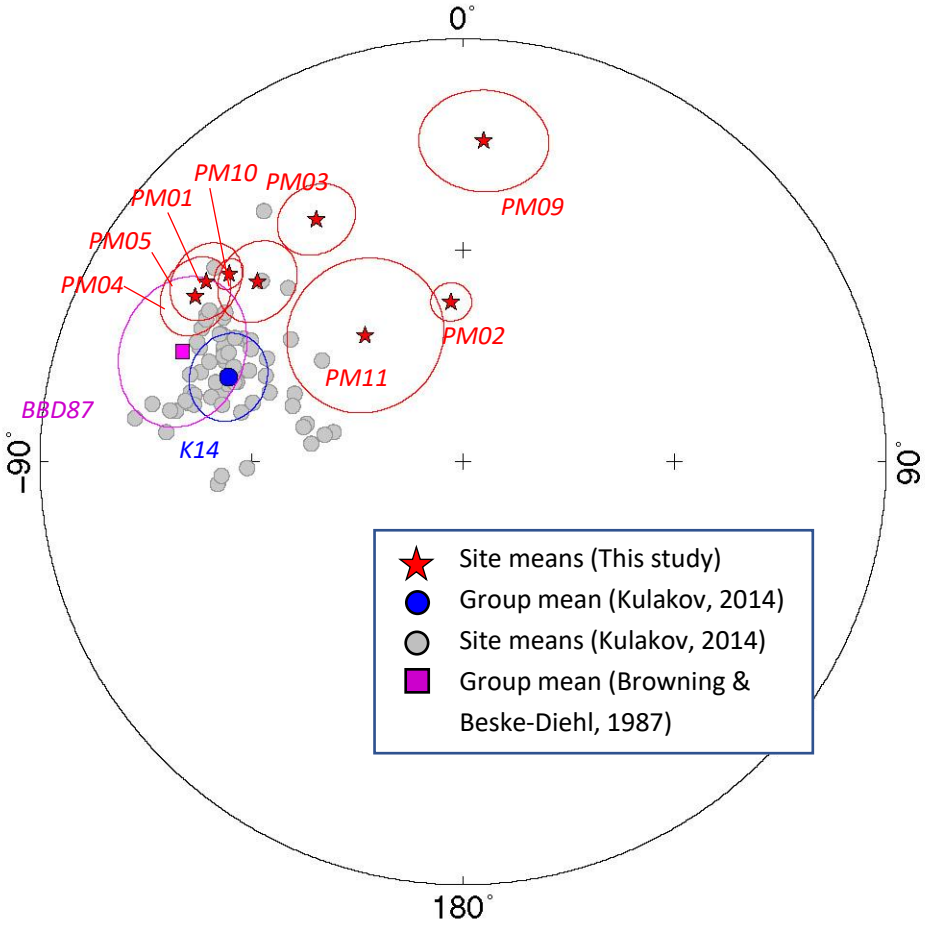

Figure 32. Equal-area plot with a summary of paleomagnetic results. Red stars: site-mean directions and their 95% confidence circles obtained in this study; Grey circles: site-mean directions reported in Kulakov (2014); Blue circle: group-mean direction with 95% confidence circle from Kulakov (2014); Magenta square: group-mean direction with 95% confidence circle from Browning and Beske-Diehl (1987).

Site-mean directions for PM01, PM03, PM04, PM05, PM10, and PM11 plot on the northerly-declination side of the site-mean distribution reported by Kulakov (2014) (Figure 32). This reflects the fact that the data from 4-6 lava flows do not represent the full range of secular variation of the geomagnetic field. It is important to consider this limitation when using the data to estimate potential rotations around the vertical axis, as discussed below.

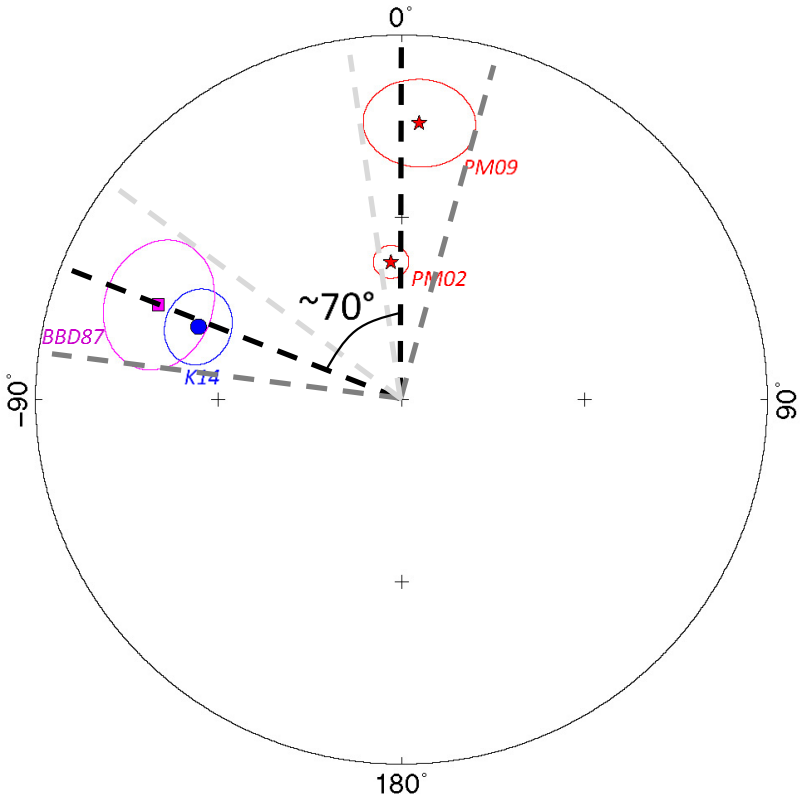

Figure 33. Site-mean paleomagnetic directions for sites PM02 and PM09 and their 95% confidence circles (red stars, circles). Group-mean directions with 95% confidence circles from Browning and Beske-Diehl (1987) (magenta square, circle) and Kulakov (2014) (blue circles). Dashed lines show an estimate of vertical-axis rotation at sites PM02 and PM09. Available data allow a 50°-105° range of possible rotation.

Paleomagnetic directions obtained from Sites PM02 and PM09 have inclinations within the range typical for PLV rocks; however, their declinations noticeably deviate clockwise from the reference directions (Figures 32 and 33). This difference in declination is unlikely to be caused by later remagnetization (see Section 3.1). A probable scenario explaining the declination difference is clockwise rotation of rocks at these sites around a vertical axis. The magnitude of rotation can be estimated by comparing site-mean declinations with the group-mean declination (D = 290°) reported by Kulakov (2014). The data suggest that rocks at Sites PM02 and PM09 could have rotated clockwise by about 70° (Figure 33). Such a rotation is generally consistent with inferred dextral strikeslip along the Keweenaw fault in this area. However, the available data allow rotation to vary within a 50° to 105° range when uncertainties are considered (Figure 33). A smaller clockwise rotation could have affected paleomagnetic directions from Sites PM03 and PM11 as they also plot slightly outside the site-mean distribution from Kulakov (2014) (Figure 32). All four potentially rotated sites (PM02, PM03, PM09, and PM11) are from the south-dipping side of the anticline, which may have a structural significance not yet understood and in need of further investigation. Additional paleomagnetic investigations of nearby sites are needed to test these hypotheses and to evaluate the amount of rotation more precisely.

Paleomagnetic data obtained from Sites PM06 and PM07 (brecciated zone along the fault segment) show randomized ChRM directions within each site. While the data do not seem to have any bearing on fault kinematics, they indicate no significant post-faulting remagnetization event that could have affected the paleomagnetic signal in the basaltic

flows of Sites PM01-05 and PM09-11. This observation lends additional confidence to the interpretations discussed above.

5.0 Conclusion

Rock magnetic and paleomagnetic results obtained in this study support the hypothesis of folding of the Portage Lake Volcanics associated with dextral strike-slip along the Keweenaw Fault system in this area. The number of samples for some sites was relatively small and the investigated area represents only a small part of the Keweenaw Fault system. Therefore, future rock magnetic and paleomagnetic investigations should include additional samples for some sites presented here as well as additional sites along the extent of the fault system. Additional samples at existing and new sites have been already collected as a part of this study and will constitute the basis for the next stage of the project. One of the most interesting results of this research that needs to be addressed further is to test the idea of vertical axis rotations along the fault using paleomagnetic declinations.

Another important outcome of this project is the demonstration that rock magnetic and paleomagnetic investigations represent a useful tool to study the tectonics of the Midcontinent Rift system at both global and regional levels.

References

Books, K. G. “Magnetization of the Lowermost Keweenawan Lava Flows in the Lake Superior Area.” U.S. Geological Survey Professional Paper, 1968, pp. 248–254.

Books, K. G. “Paleomagnetism of Some Lake Superior Keweenawan Rocks.” Professional Paper, 1972, doi:10.3133/pp760.

Bornhorst, T. J. “Tectonic Context of Native Copper Deposits of the North American Midcontinent Rift System.” Middle Proterozoic to Cambrian Rifting, Central North America, 1997, doi:10.1130/0-8137-2312-4.127.

Bornhorst, T. J., and L. D. Lankton. “Copper Mining: A Billion Years of Geologic and Human History.” Michigan Geology and Geography, 2009, pp. 150–173.

Bornhorst, T. J., et al. “Age of Native Copper Mineralization, Keweenaw Peninsula, Michigan.” Economic Geology, vol. 83, no. 3, 1988, pp. 619–625., doi:10.2113/gsecongeo.83.3.619.

Browning, T. D., and S. J. Beske-Diehl. “Paleomagnetism and the Age of Copper Mineralization in the Portage Lake Volcanics, Upper Peninsula, Michigan.” Canadian Journal of Earth Sciences, vol. 24, no. 12, 1987, pp. 2396–2404., doi:10.1139/e87-225.

Butler, R. F. Paleomagnetism: Magnetic Domains to Geologic Terranes. Blackwell Scientific, 1992.

Cannon, W. F. “Closing of the Midcontinent Rift-A Far—Field Effect of Grenvillian Compression.” Geology, vol. 22, no. 2, 1994, p. 155., doi:10.1130/0091-7613(1994)0222.3.co;2.

Cannon, W. F., and S. W. Nicholson. “Geologic Map of the Keweenaw Peninsula and Adjacent Area, Michigan.” United States Geological Survey, 2001, doi:10.3133/i2696.

Cannon, W. F., et al. “The North American Midcontinent Rift beneath Lake Superior from Glimpce Seismic Reflection Profiling.” Tectonics, vol. 8, no. 2, 1989, pp. 305–332., doi:10.1029/tc008i002p00305.

Cornwall, H. R. Bedrock geology of the Lake Medora quadrangle, Michigan: USGS Geologic Quadrangle Map GQ-52, scale 1:24,000, 1954.

Davis, D. W., and J. B. Paces. “Time Resolution of Geologic Events on the Keweenaw Peninsula and Implications for Development of the Midcontinent Rift System.” Earth and Planetary Science Letters, vol. 97, no. 1-2, 1990, pp. 54–64., doi:10.1016/0012-821x(90)90098-i.

Davis, D. W., and J. C. Green. “Geochronology of the North American Midcontinent Rift in Western Lake Superior and Implications for Its Geodynamic Evolution.” Canadian Journal of Earth Sciences, vol. 34, no. 4, 1997, pp. 476–488., doi:10.1139/e17-039.

Davis, D. W., and R. H. Sutcliffe. “U-Pb Ages from the Nipigon Plate and Northern Lake Superior.” Geological Society of America Bulletin, vol. 96, no. 12, 1985, p. 1572., doi:10.1130/0016-7606(1985)962.0.co;2.

Day, R., et al. “Hysteresis Properties of Titanomagnetites: Grain-Size and Compositional Dependence.” Physics of the Earth and Planetary Interiors, vol. 13, no. 4, 1977, pp. 260–267., doi:10.1016/0031-9201(77)90108-x.

Degraff, J. M. “Keweenaw Fault Geometry, Secondary Structures, and Slip Kinematics along the Bête Grise Bay Shoreline.” Final Technical Report, 2018, doi:10.1130/abs/2018am-321079.

Dubois, P. M. “Paleomagnetism and Correlation of Keweenawan Rocks.” Geological Survey of Canada, 1962, doi:10.4095/100589.

Ernst, R. E., and K. Bell. “Large Igneous Provinces (LIPs) and Carbonatites.” Mineralogy and Petrology, vol. 98, no. 1-4, 2010, pp. 55–76., doi:10.1007/s00710-009-0074-1.

Foucher, M. S. “Probing the Precambrian Geodynamo: Analysis of the Geomagnetic Field Behavior and Calibration of Pseudo-Thellier Paleointensity Method.” Ph.D. Thesis Michigan Technological University, 2018, p. 177.

Graham, C. D. “High-Sensitivity Magnetization Measurements.” Journal of Materials Science and Technology, 2000, pp. 97–101.

Green, J. C., et al. “Keweenawan Dykes of the Lake Superior Region: Evidence for Evolution of the Middle Proterozoic Midcontinent Rift of North America.” Geological Association of Canada, pp. 289–302.

Heaman, L. M., et al. “Further Refinement to the Timing of Mesoproterozoic Magmatism, Lake Nipigon Region, Ontario.” Canadian Journal of Earth Sciences, vol. 44, no. 8, 2007, pp. 1055–1086., doi:10.1139/e06-117.

Hirt, A. M., et al. “Thermal Generation of Ferromagnetic Minerals from Iron-Enriched Smectites.” Geophysical Journal International, vol. 115, no. 3, 1993, pp. 1161–1168., doi:10.1111/j.1365-246x.1993.tb01518.x.

Hnat, J. S., et al. “Primary Curvature in the Mid-Continent Rift: Paleomagnetism of the Portage Lake Volcanics (Northern Michigan, USA).” Tectonophysics, vol. 425, no. 1-4, 2006, pp. 71–82., doi:10.1016/j.tecto.2006.07.006.

Huber, N. K. “The Geologic Story of Isle Royale National Park.” United States Geological Survey, 1975, doi:10.3133/b1309.

Huber, N. K. “The Portage Lake Volcanics (Middle Keweenawan) on Isle Royale, Michigan.” Professional Paper, 1973, doi:10.3133/pp754c.

Hutchinson, D. R., et al. “Keweenaw Hot Spot: Geophysical Evidence for a 1.1 Ga Mantle Plume Beneath the Midcontinent Rift System.” Journal of Geophysical Research, vol. 95, no. B7, 1990, doi:10.1029/jb095ib07p10869.

Kirschvink, J. L. “The Least-Squares Line and Plane and the Analysis of Palaeomagnetic Data.” Geophysical Journal International, vol. 62, no. 3, 1980, pp. 699–718., doi:10.1111/j.1365-246x.1980.tb02601.x.

Kosterov, A. A., and M. Prévot. “Possible Mechanisms Causing Failure of Thellier Paleointensity Experiments in Some Basalts.” Geophysical Journal International, vol. 134, no. 2, 1998, pp. 554–572., doi:10.1046/j.1365-246x.1998.00581.x.

Kulakov, E. V., et al. “Paleomagnetism of ~1.09 Ga Lake Shore Traps (Keweenaw Peninsula, Michigan): New Results and Implications.” Canadian Journal of Earth Sciences, vol. 50, no. 11, 2014, pp. 1085–1096., doi:10.1139/cjes-2013-0003.

Li, H., and S. J. Beske-Diehl. “Low-Temperature Metamorphism and Secondary Components in the Portage Lake Volcanics: A Reassessment.” Canadian Journal of Earth Sciences, vol. 30, no. 7, 1993, pp. 1404–1414., doi:10.1139/e93-121.

Longo, A. A. “A Correlation for a Middle Keweenawan Flood Basalt: the Greenstone Flow, Isle Royale and Keweenaw Peninsula.” Ph.D. Thesis Michigan Technological University, 1984, p. 198.

Michels, A. C. “Paleomagnetic Study of the Portage Lake Volcanics Exposed in the Quincy Mine.” Journal of Earth Sciences, 2013.

Nicholson, S. W., et al. “Rift-Wide Correlation of 1.1 Ga Midcontinent Rift System Basalts: Implications for Multiple Mantle Sources During Rift Development.” Canadian Journal of Earth Sciences, vol. 34, no. 4, 1997, pp. 504–520., doi:10.1139/e17-041.

Ojakangas, R. W., et al. “The Mesoproterozoic Midcontinent Rift System, Lake Superior Region, USA.” Sedimentary Geology, vol. 141-142, 2001, pp. 421–442., doi:10.1016/s0037-0738(01)00085-9.

Paces, J. B. “Magmatic Processes, Evolution and Mantle Source Characteristics Contributing to the Petrogenesis of Midcontinent Rift Basalts: Portage Lake Volcanics, Keweenaw Peninsula, Michigan.” Ph.D. Thesis Michigan Technological University, 1988.

Paces, J. B., and J. D. Miller. “Precise U-Pb Ages of Duluth Complex and Related Mafic Intrusions, Northeastern Minnesota: Geochronological Insights to Physical, Petrogenetic, Paleomagnetic, and Tectonomagmatic Processes Associated with the 1.1 Ga Midcontinent Rift System.” Journal of Geophysical Research: Solid Earth, vol. 98, no. B8, 1993, pp. 13997–14013., doi:10.1029/93jb01159.

Platt, R. G. “The Marathon Dikes. I: Zirconium-Rich Titanian Garnets and Manganoan Magnesian Ulvöspinel-Magnetite Spinels.” American Mineralogist, 1979, pp. 546–550.

Schmidt, P. W. “Palaeomagnetic Cleaning Strategies.” Physics of the Earth and Planetary Interiors, vol. 76, no. 1-2, 1993, pp. 169–178., doi:10.1016/0031-9201(93)90066-i.

Silver, L. T., et al. “Precambrian Formations and Precambrian History in Cochise County, Southeastern Arizona, in Callender.” New Mexico Geological Society, 1978, pp. 157–163.

Smirnov, A. V., et al. “Evolving Core Conditions Ca. 2 Billion Years Ago Detected by Paleosecular Variation.” Physics of the Earth and Planetary Interiors, vol. 187, no. 3-4, 2011, pp. 225–231., doi:10.1016/j.pepi.2011.05.003.

Smirnov, A. V., et al. “Temperature Dependence of Magnetic Susceptibility as a Potential Indicator of Fine-Scaleoxyexsolution in Igneous Rocks, Eos Trans.” AGU, 86(52), Fall Meet. Suppl., Abstract GP13A-0040, 2015.

Tarduno, J. A., and A. V. Smirnov. “The Paradox of Low Field Values and the Long-Term History of the Geodynamo, in Timescales of the Paleomagnetic Field.” Geophysical Monograph Series, vol. 145, 2013, pp. 75–84., doi:10.1029/145gm06.

Tauxe, L., et al. “Potbellies, Wasp-Waists, and Superparamagnetism in Magnetic Hysteresis.” Journal of Geophysical Research: Solid Earth, vol. 101, no. B1, 1996, pp. 571–583., doi:10.1029/95jb03041.

Tyrrell, C. W., et al. “Keweenaw Fault Geometry and Kinematics along Bête Grise Bay, Michigan: Institute on Lake Superior Geology.” 64th Annual Meeting, Iron Mountain, Proceedings, vol. 64, 2018, pp. 106–107.

Verwey, E. J. “Electronic Conduction of Magnetite (Fe3O4) and Its Transition Point at Low Temperatures.” Nature, vol. 144, no. 3642, 1939, pp. 327–328., doi:10.1038/144327b0.

Vincenz, S. A., and K. Yaskawa. “Phenomenon of Partial Self-Reversal in Keweenawan Rocks: 2. Magnetization of Upper Keweenawan Lavas and Sediments and of Lower Keweenawan Dikes.” Journal of Geophysical Research, vol. 73, no. 8, 1968, pp. 2753–2767., doi:10.1029/jb073i008p02753.

White, W. S. “The Keweenawan Lava of Lake Superior, an Example of Floodbasalts.” American Journal of Science, 1960, pp. 367–374.